Università degli Studi della Basilicata

Scuola di Scienze Agrarie, Forestali, Alimentari ed Ambientali

Agricultural, Forest and Food Sciences PhD Program

Curriculum: Agriculture, Forest and Environmental Sciences

Academic Discipline: AGR/08 - Agricultural hydraulics and watershed protection

Cycle XXXV

Title of the Dissertation

"Comparing canopy-scale actual transpiration fluxes of a tomato crop as measured in the field and estimated by an agro-hydrological model"

Tutor
Prof. Antonio Coppola

Co-tutor
Prof. Eng. Alessandro Comegna

Dr. Raffaella Maria Balestrini (CNR-IPSP)

PhD student
Ameneh Sobhani

PhD Coordinator
Prof. Giovanni Carlo Di Renzo

Academic Year **2022/2023**

Acknowledgment

First of all, I wish to thank Eni S.p.A. (Ente Nazionale Idrocarburi) for granting me the Study Scholarship. The funding made it possible to carry out this project at the location in Metaponto, turning this degree project into an invaluable once in a lifetime experience.

I also wish to thank my supervisor Professor Antonio Coppola, and my co-supervisors: Professor Alessandro Comegna, from the School of Agriculture, Forest, Food and Environmental Sciences (SAFE), University of Basilicata, and Dr. Raffaella Balestrini, from Italian National Research Council, for all technical and scientific support throughout the whole research project and Dr. Giovanni Marino for providing the eco-physiological data.

Last, I wish to show the deepest gratitude to Dr. Giovanna Dragonetti from Mediterranean Agronomic Institute, Land and Water Division (IAMB) in Bari, and Dr. Shawkat Basel Mostafa Hassan, from the School of Agriculture, Forest, Food and Environmental Sciences (SAFE), University of Basilicata, for being so helpful during three years. All the results from the laboratory and field site would have been impossible to obtain if it was not for them.

Contents

List of figures

List of tables

List of symbols

Acronyms

SHP	Soil hydraulic properties
$T_{a,m}$	macroscopic root uptake approach
LAI	Leaf-Area Index
$T_{a,l}$	Single-leaf transpiration rates
$T_{a,c}$	The canopy-scale transpiration
MLR	Multiple Linear Regression
θ_s	saturated water content
n	slope of the water retention curve
T_a	actual transpiration
RE	Richards' equation
θ (h)	soil water-pressure head
T_p	potential transpiration
S_p	potential water uptake in each node
S_a	actual water uptake in each node/ actual sink term
g(z)	root density distribution
Gc	canopy conductance
k	extinction coefficient
SPAC	Soil-Plant-Atmosphere Continuum
J_w	water flux density
$\frac{\Delta\Psi_t}{\Delta x}$	total water potential gradient
K	unsaturated hydraulic conductivity
Ψ_t	total water potential
Ψ_o	sum of osmotic
Ψ_m	matric or pressure
Ψ_g	gravitational
MPa	megapascals
gs	stomatal conductance
C(h)	soil water capacity
h [cm]	soil water pressure head
h_o [cm]	osmotic head

t [d]	time
z [cm]	vertical coordinate being positive upward
K(h)	hydraulic conductivity
ET_p	potential evapotranspiration
DI	deficit irrigation
IRGAs	infrared gas analyzers
TDR	time domain reflectometry
θ_{TDR}	water contents measured by the TDR probe
θ_{2D}	average water content predicted by the 2D model
V_0	air volume flow rate
STP	standard temperature and pressure conditions
W	mass flow of air
e_{in}	partial pressures of water vapor entering
e_{out}	partial pressures of water vapor exiting
$W_{vapor,in}$	water vapor's molar flow rate
P	atmospheric pressure.
Dt	difference between leaf and air temperatures
λ	latent heat by vaporization of water
M_a	air molecular weight
C_p	specific heat at constant pressure,
r_b	boundary layer resistance to vapor transfer
σ	Stefan Boltzmann constant
t_c	cuvette temperature.
t_{leaf}	leaf temperature
e_{leaf}	saturation vapor pressure
g_{total}	total conductance
r_s	stomatal resistance
r_b	boundary resistance
C_{in}	concentrations entering
C_{out}	concentrations exiting
FLOWS-HAGES	Flow of Water and Solutes in Heterogeneous Agricultural and Environmental Systems
t (T)	time
z (L)	vertical coordinate being positive upward
$S_w(h)$	sink term describing water uptake by plant roots

S_e	effective saturation
h	soil water potential
θ	soil water content
θ_s	water content at saturation
θ_r	residual water content
α_{VG}, n and m	shape parameters.
K_0	saturated hydraulic conductivity
τ	parameter to account for tortuosity
D_r	the root depth.
α_{rw}	reduction coefficient

Abstract

Root water uptake, and subsequently transpiration, is a main component of the hydrological cycle and, hence, a main input to hydrological models. Transpiration rates can be either measured in the field at leaf and/or canopy scale or can be estimated using numerical modelling with either microscopic or macroscopic approaches. The main purpose of this study is to compare the transpiration rates measured at the leaf scale and those calculated by a macroscopic approach embedded into the Agro-hydrological model FLOWS under variable soil properties and water availability. For this purpose, sixteen plots were cultivated with tomato crops in Metaponto Area in South Italy. Of those plots, 8 plots were irrigated with 100% of the potential evapotranspiration, ET_p, (hereafter, the control group), and 8 plots were irrigated with 80% of ET_p (hereafter, the Deficit Irrigation group or DI group). Soil Hydraulic Properties (hereafter, SHP) were collected using a new fast field measurement based on the infiltration from a point source. Leaf-Area Index, LAI, was also measured in situ using a leaf-area meter. The crop coefficients, K_c, were estimated from LAI based on the literature for tomato crops in Southern Italy. The daily macroscopic transpiration rates, $T_{a,m}$, were obtained using FLOWS Agro-hydrological model, which is based on solving one-dimensional Richards Equation (RE), using the soil and vegetation data. The leaf-scale stomatal conductance, $g_{s,l}$, and transpiration rates, $T_{a,l}$, were measured in the field using the infrared Gas Analyzers (IRGA). For the sake of comparison with the macroscopic transpiration rates, $g_{s,l}$ was upscaled to canopy scale stomatal conductance, $g_{s,c}$, by the big-leaf approach using LAI and an extinction factor accounting for radiation attenuation. Then, the canopy-scale transpiration rates, $T_{a,c}$, were obtained by the well-known Penman-Monteith equation using the $g_{s,c}$. Multiple Linear Regression, MLR, was used to find the statistical correlation among transpiration rates (both $T_{a,m}$ and $T_{a,c}$), the SHP and $g_{s,c}$, The results emphasize the strength of the model as it smooths the spatial variability of transpiration rates reducing the uncertainties resulting from the erratic variabilities coming from leaf-scale measurements as well as the ability of the model to obtain the daily transpiration rates along the whole growth season, which are difficult to obtain from leaf-scale measurements. The results also showed the important role of SHP in transpiration rates. Both $T_{a,m}$ and $T_{a,c}$ are strongly affected by the saturated water content, θ_s, and the slope of the water retention curve, n_{vG}. In addition, a reduction in transpiration rates was observed in the whole DI group and even in a plot in the control group. The stress experienced in the latter plot was due to the SHP and proved that stress periods can occur even when providing the roots with 100% of ET_p.

Keywords; Soil Hydraulic Properties, Agrohyrological model, TDR-2D method, Flows-Hages Model, Actual transpiration rates

Chapter 1

1. Introduction

1.1. Problem position

Water uptake by plant roots is a key component of the soil hydrological balance and is of concern for a range of hydrological, agricultural and ecological applications because it contributes, either directly or indirectly, to the partitioning of infiltrated water into evaporation, transpiration and deep percolation fluxes. Water uptake by plant roots greatly influences the transport of water and chemicals (e.g., nutrients) in soil-plant systems. This transport process has critical effects on crop yields, as well as the quality and quantity of groundwater recharge under croplands (Wallach and van Genuchten, 1990; Schmidhalter *et al.*, 1994). Through water uptake and transpiration in general, plants play a key role in the Earth system by linking the water and the carbon cycle between soil and atmosphere (Feddes *et al.*, 2001; Eviner and Stuart Chapin, 2002; Feddes, 2004; Asbjornsen *et al.*, 2011).

Root uptake is a dynamic process influenced by soil chemical-physical and biological features, plant and climate conditions. It depends on a number of factors such as soil conditions (e.g., soil water pressure head and hydraulic conductivity), osmotic head (in saline condition), evaporative demand, root properties (e.g., rooting depth and root density distribution) and canopy properties. Understanding root water uptake is substantial to understand plant-soil-water relations and thus ecosystem functioning, in particular efficient plant water use, storage keeping and competition in ecosystems (Davis and Mooney, 1986; Le Roux *et al.*, 1995; Jackson *et al.*, 1996; Hildebrandt and Eltahir, 2007; Arnold and Mcdonald, 2009; Meißner *et al.*, 2014).

The root uptake integrated along the whole root zone gives what is called actual transpiration, T_a. Actual transpiration by the plants, T_a, is a crucial component of the water balance. It involves stomatal diffusion of water taking place jointly with carbon dioxide exchange and is thus strictly connected to vegetation biomass yield. At the leaf scale, the transpiration process is controlled by the response of stomata to physiological and environmental factors such as irradiance, the temperature of the leaf,

atmospheric water vapour pressure gradients and CO_2 concentration (Cowan and Farquhar, 1977; Buckley and Mott, 2002). The single leaf transpiration may be measured by devices specifically designed for measuring gas exchanges (for example, PP Systems, 2017). In a single plant, sap flow measurements remain a reference tool for measuring transpiration.

However, the influence of the different environmental and physiological factors controlling transpiration at the canopy level can only be evaluated through mathematical modelling. A crucial issue is to develop a model which accounts for all the factors controlling stomatal conductance.

Many models exist looking for a description of stomatal control of water and CO_2 fluxes at the leaf-scale, some more focused on physiological aspects (for example, Leuning, 1995), some emphasising more the role of soil, plant and atmospheric processes on water and CO_2 fluxes (Williams *et al.*, 1996; Baldocchi and Meyers, 1998; Dewar, 2002). For example, the response of stomatal conductance to environmental and physiological variables have been modelled by Jarvis *et al.* (1976) through a semi-empirical model relating stomatal conductance to irradiance, the temperature of the leaf, as well as soil water pressure head.

Relating leaf to canopy transpiration is not a simple task as it generally involves scaling up leaf-scale stomatal conductance measurements to the canopy scale. While leaf stomatal conductance and other factors controlling evapotranspiration are relatively easy to measure, estimating canopy conductance requires complex mechanistic or empirical approaches (Jarvis and McNaughton, 1986; Shuttleworth, 2007). A common approach is the so-called "big-leaf" model, where the canopy is considered as a "macro-leaf whose conductance is obtained by scaling the leaf-scale stomatal conductance though the leaf area index (LAI), by accounting for an extinction factor. Another approach is the so-called dual-source model proposed by Shuttleworth and Wallace (1985), which separately estimates evaporation and transpiration and accounts for the biophysical and hydrological processes occurring within the canopy. However, the model involves complex parameterization and has been mostly used in simplified versions, which limits the strength of the model (Brisson *et al.*, 1998; Li *et al.*, 2010).

The big-leaf assumption itself does not take appropriately into account the complex structure of the canopy, where the leaf distribution, which affects the transpiration fluxes from the canopy, changes with canopy heights and leaf angles (Baldocchi and Meyers, 1998). And yet, many studies have proven the practical validity of the big-leaf approach (Moran *et al.*, 1996; Mu *et al.*, 2011; Monteith and Unsworth, 2013). The well-known and consolidated Penman-Monteith equation, estimating evapotranspiration (evaporation plus transpiration) at canopy scale, is based on the big-leaf approach to calculate the canopy conductance ($g_{s,c}$) required by the equation (Monteith and Unsworth, 2013). Canopy scale transpiration is an essential input for agro-hydrological models, which are more and more used for applications at the field or larger scales. The hydrological component of dynamics, physically based agro-hydrological models generally rely on mechanistic descriptions of water flow (and solute transport) in soils (Van Dam *et al.*, 1997; Abrahamsen and Hansen, 2000; Šimůnek *et al.*, 2008; Coppola *et al.*, 2019). Richards' equation (RE) is generally used for water flow and requires the soil water-pressure head, $\theta(h)$, and hydraulic conductivity-water content, $K(\theta)$, functions as an input. Generally, RE has to be solved numerically by dividing the flow fields in several simulation compartments where the equation has to be solved with either finite differences or finite elements methods. Frequently, when these models have to be used at applicative scales (field-scale, for example), they use a macroscopic approach for root uptake, so that potential transpiration, T_p, is distributed over the numerical simulation nodes in the whole root zone proportionally to root density (Feddes *et al.*, 1978; Feddes, 2004), to evaluate the potential water uptake in each node, S_p. To calculate the actual water uptake in each node, S_a, S_p is eventually reduced in the case of water and salinity stresses, whose presence is evaluated based on soil water content and salinity in each simulation node (Molz, 1981). S_a is thus included in the RE as a so-called sink term. Integrating S_a over the root zone provides the T_a calculated by the model, hereafter $T_{a,m}$. The macroscopic approach does not describe dynamically and in detail the plant and its root system. It neglects the effects of the root geometry and flow pathways around roots. With this approach, the root system is rather modeled in a static way and just represents a pump drawing water from different soil compartments according

to a given root distribution, *g(z)*. The characteristics of the aerial part of the plant are generally given as leaf area index, *LAI*, and leaves distribution is just described through an extinction coefficient, *k*, for solar radiation within the canopy. Both *g(z)*, *LAI* and *k* have to be provided as input to the model. There are also microscopic approaches focusing on descriptions of radial flow to, and uptake by, individual roots and its transpiration through leaves stomata (Hillel *et al.*, 1975; Roose and Fowler, 2004; Schröder *et al.*, 2008). In any case, because of the complexity of the roots' geometry and the flow equations into and through each rootlet, the application of the microscopic approach is still limited to the scale of a single plant and is not considered in this study.

The macroscopic sink term's variability results from the variability of the soil-water pressure and the osmotic potentials in the different simulation nodes in the root zone (Coppola *et al.*, 2015). Thus, as discussed by Coppola at al. (2015), the T_a calculated by a macroscopic approach in Agro-hydrological models may be significantly impacted by the spatial and temporal variability of the water content (and salinity) in the root zone across a field. The water content variability in the root zone, in turn, is strictly related to the natural variability of the soil hydraulic properties.

However, it is not clear to which extent the spatial variability of hydraulic properties also impacts the actual transpiration at the leaf scale. Moreover, there are still issues deserving to be clarified, concerning, on one side, the relationship between actual transpiration measured at the microscopic leaf scale and that calculated by a macroscopic approach at the canopy scale and, on the other side, the role of the spatial variability of soil hydraulic properties on both the leaf scale and canopy scale actual transpiration.

1.2 Objectives of the thesis

In the literature, there is plenty of approaches for either measuring or estimating actual transpiration at different scales. However, there is still a need to better understand the relationship between the transpiration rates at microscopic and macroscopic scales, as well as the relationship between soil hydraulic properties' spatial variability and the transpiration rates at different scales.

To partially fill the gap, the purpose of this thesis was to compare the actual transpiration, as measured at leaf scale and estimated by a macroscopic approach in an Agro-hydrological model, under variable soil properties and water availability. For this purpose, sixteen plots were cultivated with tomato crops, of which eight plots were fully irrigated, and eight plots were irrigated under deficit irrigation, DI, by applying 80% of the potential evapotranspiration, ET_p. The soil hydraulic parameters were obtained by a fast hydraulic characterization method, hereafter called TDR-2DM method (Coppola et al., 2022). The microscopic transpiration rates, stomatal conductance and photosynthesis were measured from single leaves of different plots using a combined system of infra-red gas analyzers (IRGAs), while the macroscopic transpiration fluxes were calculated for all sixteen plots using FLOWS-HAGES physically-based Agro-hydrological model (Coppola *et al.*, 2019).

For the comparison, the T_a measured at leaf scale was firstly converted to canopy scale actual transpiration, hereafter $T_{a,c}$, by using the big-leaf approach. Then, physical explanations were given for interpreting the behavior observed in the $T_{a,c}$ and that calculated by the macroscopic model, $T_{a,m}$. A multiple linear regression, MLR, was finally used to find the possibility of predicting $T_{a,c}$ and $T_{a,m}$ from the stomatal conductance, as well as, the soil hydraulic parameters.

1.3 Physical and Physiological aspects of root water uptake

The rate at which a plant uptakes water (transpires) depends upon the water transmission rates at different levels in the soil-plant-atmosphere continuum: (1) The rate at which water is transmitted through the soil to the plant root; (2) The rate at which water is absorbed from the soil by the plant root and transmitted to the vaporization sites within the leaves; and (3) The rate at which water is

transmitted from the vaporization sites within the leaves to the atmosphere. The successive transport of water through the soil, root cells, plant xylem, leaf cells, and into the atmosphere is considered to be a “catenary process” (Molz et al., 1968).

The effect of any of the three processes on transpiration can be studied by assuming that the other two processes are capable of transmitting water at an unlimited rate. In this sense, Cowan (1965) defines the term potential transpiration as the rate of transpiration that would be sustained by a specified cropped area under given environmental conditions if the leaves of the crop were fully turgid. In other words, it is assumed that the soil and plant are capable of transmitting to the sites of vaporization within the leaves any quantity of water that can be evaporated from the leaves and transmitted to the atmosphere. Thus, potential transpiration is a measure only of the rate at which water can be transmitted from the leaves to the atmosphere unrestrained by the rest of the system. It is potential transpiration that limits actual transpiration under such conditions.

Because plant impedance is small, we may consider the transpiration rate of a plant to be limited by potential transpiration under moist soil conditions and by potential soil-moisture availability under dry soil conditions but not by the capacity of the plant to transmit moisture from the root to the leaves. A plant transpires at the potential transpiration rate as long as that rate is less than the potential soil-moisture availability. In such a case, transpiration is limited by the capacity of water to move from the leaves to the atmosphere. This condition may occur when potential soil-moisture availability is large because the soil is wet, or when potential transpiration is small due to cold humid weather. A plant transpires essentially at the rate of potential soil-moisture availability if that rate is less than the potential transpiration. In such a case, transpiration is limited by the capacity of water to move through the soil to the root. Under these conditions, a transient situation occurs in which the moisture movement out of the plant and into the atmosphere exceeds the moisture movement through the soil to the root. The decrease in moisture storage causes biological changes in the plant that leads to wilting. If the loss in moisture storage in the plant exceeds a certain value, permanent wilting occurs.

1.4 Flow of water from the soil to the roots and plant vascular system

Water is transported through the soil into the roots and plant xylem towards the plant canopy where it eventually transpires into the atmosphere. In a macroscopic sense, water transport within this Soil-Plant-Atmosphere Continuum (SPAC) can occur only if the water flow is continuous between the soil rooting zone and the plant atmosphere. Conceptually, water transport is mathematically described by an Ohm's Law type of relationship, expressing the flux or mass flow rate of water (M L-2 T-1) as a function of a driving force (water potential *per* unit distance), and a proportionality factor that defines the ability of the transmitting medium to conduct water. In soil science, this relationship is known as Darcy's law (Darcy, 1856), and its modified form is widely accepted as a means to predict water flow in unsaturated soils from (Buckingham, 1907):

$$J_w = -K\frac{\Delta\Psi_t}{\Delta x} \qquad \text{(Equation)}$$

where Jw denotes water flux density (LT-1), $\frac{\Delta\Psi_t}{\Delta x}$ is defined as the total water potential gradient (LL-1), and K is known as the unsaturated hydraulic conductivity (LT-1).

Equation 1 states that the water flow rate is constant with time at any spatial location within SPAC, i.e., the flow must be at some kind of dynamic equilibrium. In contrast, flow is most often transient, i.e., fluxes change with time. Nevertheless, the steady state expression can still be applied as long as the time period over which it is used is short, compared to the rate at which the changes in time occur. In SPAC, the driving force for water to flow is the gradient in total water potential (ψt).

Soil water potential is formally defined as (Aslyng, 1963): " the amount of work that must be done per unit quantity of pure water in order to transport reversibly (independent of the path taken) and isothermally to the soil water at a considered point, an infinitesimal quantity of water from a reference pool. The reference pool is at the elevation, the temperature, and the external gas pressure of the considered point, and contains a solution identical in composition to the soil water at the considered point." In other words, the water potential is decreased if the water is at a lower elevation, lower

temperature, lower pressure or, for water solutions, with increasing solute concentrations. The total potential of bulk soil and plant water can then be described as the sum of all possible component potentials, so that the total water potential (Ψ_t) is equal to the sum of osmotic (Ψ_o), matric or pressure (Ψ_m) and gravitational (Ψ_g)

$$\Psi_t = \Psi_o + \Psi_m + \Psi_g \quad (1)$$

This additive property of water potential is based on the assumption that water is in thermal equilibrium and that physical barriers within SPAC behave as perfect semi-permeable membranes. The negative water potential is effectively the result of suction forces on the water solution towards the solid soil or plant cell surface, so it is often conveniently denoted by a positive suction force.

Structure of roots and pathways of water in the root system

Although variable in size between monocotyledons and dicotyledons, the general structure of root apices is broadly similar for many plants (Russell, 1977) (see Figure 1). They contain the vascular stele and root cortex (Figure 1). The inner center contains the stele, which comprises the vascular system (xylem and phloem) and the associated ground tissue (pericycle; interfascicular regions, and pith, if it occurs). The cortex consists of the inner endodermis, cortex, and hypodermis and is bounded by an outer layer of epidermal cells from where root hairs develop. A prominent feature of the primary structure of most roots is the endodermis, the inner layer of cells of the cortex which separates it from the stele. The endodermis is not part of the stele. Early in the development of the endodermis, suberin (a fatty substance) is deposited in bands on the transverse walls and radial walls in the longitudinal direction, forming the Casparian strip. Roots are in contact with the surrounding soil by a film on its surfaces or mucigel which can also play a controlling role on water and nutrient absorption by the plant.

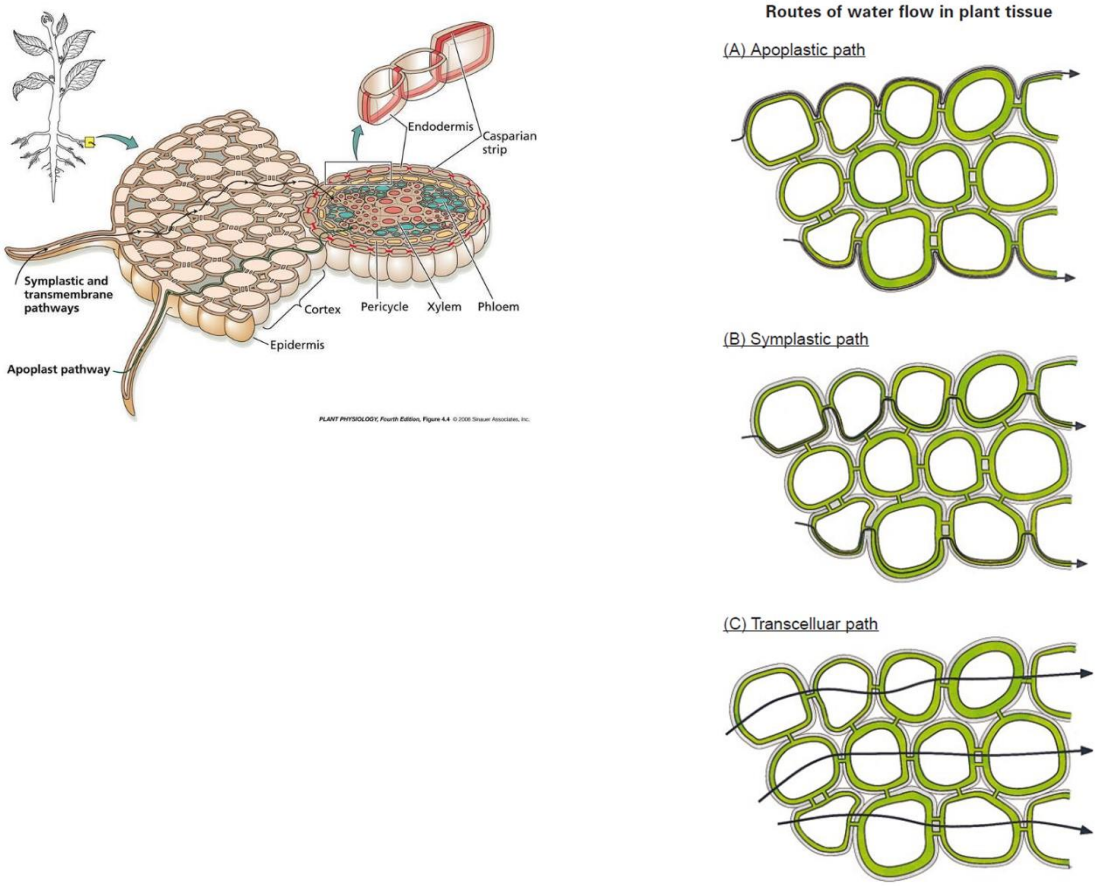

Figure 1. Radial composition of a thin root and different routes of water flow in the plant tissues

The radial pathways for water and nutrients in roots are either intracellular (apoplastic) and/or intercellular (symplastic pathway) (Steudle and Peterson, 1998). Figure 1 provides a schematic view of the routes of water flow in plant tissue. The tissue is represented by four cell layers arranged in series. (A) Denotes the apoplastic path (cell walls, grey) around protoplasts. The symplastic path (B) is mediated by plasmodesmata which bridge the cell walls between adjacent cells so that a cytoplasmic continuum is formed (green). During the passage along the apoplast and symplast, no membranes have to be crossed. On the transcellular path (C), two plasma membranes have to be crossed per cell layer. The transcellular path is used especially by water which has a high membrane permeability. Usually, this component is negligible for solutes. Note that symplastic and transcellular flow components cannot be separated experimentally and are summarized as a cell-to-cell components of water flow. Due to the rapid water exchange between protoplasts and adjacent

apoplast, there should be local water flow equilibrium between the two compartments at any time. In the root, the apoplastic flow component is modified by the existence of apoplastic barriers (Casparian bands). These are usually thought to be completely impermeable for water and solutes (including nutrient ions).

1.5 The flow of water in the plant vascular system

Once the water enters radially into the thinner roots and their xilematic vessels, axial movement takes place. Again, water potential gradients serve as the force inducing flow within and between adjacent compartments in the plant to the atmosphere (Boyer, 1995; van der Ploeg et al., 2008). Figure 2 highlights the typical potential differences between soil water and atmospheric water vapor, oftentimes amounting to tens of megapascals (MPa).

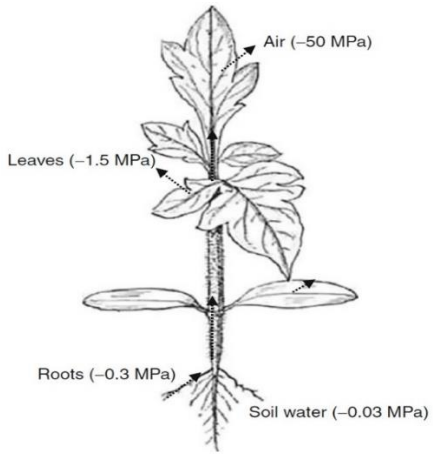

Figure 2. The transpiration stream through the soil–plant– atmosphere continuum (SPAC), with representative potential values indicated for various compartments

The effectiveness of plants in meeting a continuous evaporative demand through increased water extraction is primarily determined by the soil's ability to deliver water to the root surface. As the soil dries, the soil water potential decreases, leading to a subsequent reduction in hydraulic conductivity. To maintain the water potential gradient powering the transpiration stream, the root water potential must decrease beyond that of the soil. But while the soil water potential can decrease to very low values, the root water potential is limited by a critical value, around 1.6 MPa for most agricultural

crops (Koorevaar et al., 1983), below which plant death ensues. An Ohm's law type of relationship (Van den Honert, 1948; Feddes, 2004) describes the water flow through the SPAC.

Some physiological aspects of root uptake and stomatal conductance under water stress conditions

The hydrostatic force generated in the xylem from the evaporation of water from the leaves is the main driver for root water uptake, and within the root, this force drives water movement through the intercellular spaces to the xylem (i.e., apoplastic pathway) (Steudle and Peterson, 1998). In addition, an osmotic gradient between the roots and the soil solution drives the flow of water to the root, and within the root, through the cell-to-cell pathway. When roots are exposed to drought, young roots tend to mature closer to the root tip and form barriers due to suberin and lignin deposition such as in the Casparian band (Passioura, 1988; Kreszies et al., 2018). These anatomical changes can affect the root apoplastic water flow and osmotic cell-to-cell water flow hydraulic conductivities, and their relative contributions to water uptake from an increased resistance to water movement through the apoplastic pathway, which may favor the cell-to-cell pathway (Knipfer and Fricke, 2011; Barrios-Masias et al., 2015). Changes in xylem vessel diameter can also affect the hydraulic conductance of the root system, which has been proposed as an approach to regulate crop water use under water-limited conditions (Richards and Passioura, 1989). According to the Hagen–Poiseuille equation, water flow in the xylem elements (i.e., vessel conductivity) is significantly impacted by the fourth power of the radius of the xylem vessel. As roots sense drying soils, physical and chemical signals lead to the production of abscisic acid, ABA, in roots and leaves (Jackson et al., 1996; Lambers et al., 2008). In the leaves, ABA induces changes in the turgor of the guard cells and results in the closing of the stomatal pore (Thompson et al., 2007). This can result in a partial or complete closure of the stomata to restrict water loss, a response that has been previously found in tomatoes (Thompson et al., 2007). Slight decreases in stomatal conductance (gs) have been shown to increase water use efficiency without compromising C assimilation and yields in tomatoes (Barrios-Masias and Jackson, 2016), but long-term and large reductions in stomatal conductance can result in impaired capacity for C assimilation.

1.6 Modelling approaches to root uptake

Agro-hydrological applications require a quantitative description of water uptake by plant roots. Several approaches have been proposed to model water uptake microscopically and macroscopically over the years. Comprehensive reviews from a mostly hydrological perspective were carried out (Molz, 1981; Hopmans and Bristow, 2002; Feddes, 2004; Wang and Smith, 2004). The microscopic approach generally focuses on descriptions of radial flow to, and uptake by, individual roots (Hillel et al., 1975). The approach assumes a single root to be an infinitely long cylinder of uniform radius and water-absorbing properties (Gardner, 1960). Water flow to a root was described using the Richards equation formulated in radial coordinates, with the flow into the root driven by water potential gradients between the root and surrounding soil and proportional to the hydraulic conductivity of the soil surrounding the root (Mmolawa and Or, 2000) or the root radial water conductivity parameter (Roose and Fowler, 2004). Even if such approaches are more realistic in simulating soil-root interactions at the individual root scale, they lack the relevant soil and root data and the huge computational requirements for simulation purposes at this microscopic scale. The microscopic approach (Gardner, 1960) needs detailed information on the geometry of root systems, which is practically impossible to acquire. That's why soil water flow models that consider flow to each individual rootlet or plant root architecture have been limited to applications at a relatively small scale of a single plant.

On the other hand, a macroscopic approach (Feddes type approach) is thus much more adopted in hydrologically oriented soil-plant-atmosphere continuum modelling for describing plant water uptake based on the observed response to both soil water pressure and osmotic potentials (Feddes et al., 1978; Feddes, 2004). With this approach, the potential transpiration is distributed over the root zone proportionally to root density and depth, and is locally reduced depending on soil saturation and salinity status, i.e., water and salinity stresses (Molz, 1981). It neglects the effects of the root geometry and flow pathways around roots, and formulates root water uptake using a macroscopic sink term that lumps root water uptake processes into a single term of the governing mass balance equation.

It is essentially an empirical approach and needs to be calibrated for different plants and climatic conditions. In the macroscopic approach, the root water-uptake problem is generally solved by introducing an actual sink term, Sa(h, ho) [d-1], in the Richards equation for water flow:

$$C(h)\frac{\partial h}{\partial t} = \frac{\partial}{\partial z}\left(K(h)\frac{\partial h}{\partial z} - K(h)\right) - S_a(h,h_o) \qquad (2)$$

where C(h)=dθ/dh is the soil water capacity, θ [-] is the volumetric water content, h and ho [cm] are the soil water pressure head and osmotic head, respectively, t [d] is time, z [cm] is the vertical coordinate being positive upward, and K(h) [cm d-1] the hydraulic conductivity.

A Feddes-type macroscopic sink term under water and/or osmotic stresses strictly depends on two aspects: i) the root density distribution, g(z), and ii) activity over the root zone during the growth season of a crop. Activity is used here in hydraulic terms, to express the physical dependence of root uptake on changes in the total hydraulic pressure head of soil water, which in turn affect water fluxes to the roots, thus influencing water uptake. In a Feddes-type sink term, reduced root activity is accounted for by introducing an uptake reduction α(h, ho) function depending on the local water, h, and osmotic, ho, potentials experienced by roots at any depths along the root-zone.

Databases on root system distributions exist with information on maximum rooting depth, root length densities and root biomass (Canadell et al., 1996; Jackson et al., 2000a,b among others). However, these databases lack the information on the effect of different water and salinity stresses on root distribution. This is why, in the context of water uptake comparisons among different water and salinity stresses, there is the fairly generalized practice of assuming that the root system distribution and morphology of a crop remain fixed under different stresses (Homaee et al., 2002a, 2002b; Skaggs et al., 2006a, 2006b). This is tantamount to assume that, once a root system becomes established in non-stressed conditions, increasing water and/or osmotic stresses may have effects mainly on root activity but will not significantly change the initially developed root distribution, irrespective of the strength of the stress. The stresses will only change root activity according to an uptake reduction

function characterizing the crop under specific soil and climatic conditions. Moreover, it is implicitly assumed that by removing the stress, for example by supplying adequate water amounts or leaching salts with a surplus of water, the root system will recover its previous uptake activity.

1.7 Thesis organisation

This dissertation is organized into five chapters with the relevant literature being reviewed. The introduction (Chapter 1) provides a brief overview of the complex problem concerning the integration and the introduction of prospection methods in the agronomic and experimental sites, to quantify Crop Properties, Soil Hydraulic Properties and the agro-hydrological model. This chapter also gives a description of the primary aim and objectives of the thesis.

Chapter 2 introduces and describes the experimental site and experiment setup in the field and the principles of the methods, including Soil Hydraulic characterizations, Measuring Stomatal conductance, and transpiration rates. Furthermore, this chapter explains the performance TDR-2Dmode model and the simulations by the agro-hydrological Flows-Hages model.

Chapter 3 assesses the results and discussions about the soil hydraulic parameters variabilities and Crop parameters variabilities and the simulation results (root uptake, transpiration rates), and the relationships between transpiration rates in the canopy scale, the leaf scale, and the macroscopic approach obtained by Flows-Hages model. Finally, compare simulated and measured root uptake (transpiration rates in the leaf scale, the canopy scale and the macroscopic approach). As well as illustrate the correlation between soil hydraulic parameters and crop parameters by multiple linear regression, MLR.

Chapter 4 provides the key conclusions from the study and discusses recommendations for future study developments.

Chapter 5 gives the Eventual Appendix.

Chapter 2

2. Materials and Methods

This study was conducted through a combination of field studies, laboratory results and computer modeling. Results from the field studies, along with variable soil properties, meteorological data and crop properties, were used as inputs in the Flow of Water and Solutes in Heterogeneous Agricultural and Environmental Systems (FLOWS-HAGES) model to simulate water flow and solute transport in the soil-vegetation-atmosphere system especially adjusted to the tomatoes in Metaponto area, Southern Italy.

2.1. Case study

The study site is the “Pantanello” experimental site located in the Metaponto area, southern Italy. Its geographical coordinates are 40°23′ North in latitude and 16°48′ altitude East in longitude and is 6 meters above sea level and approximately 760 m^2 in size. Topographically, the area is characterized by extremely flat terrain between two main rivers, Bradano and Basento, and situated 5.2 km from the eastern the Gulf of Taranto, about 2 km from the town of Metaponto (Figure 3).

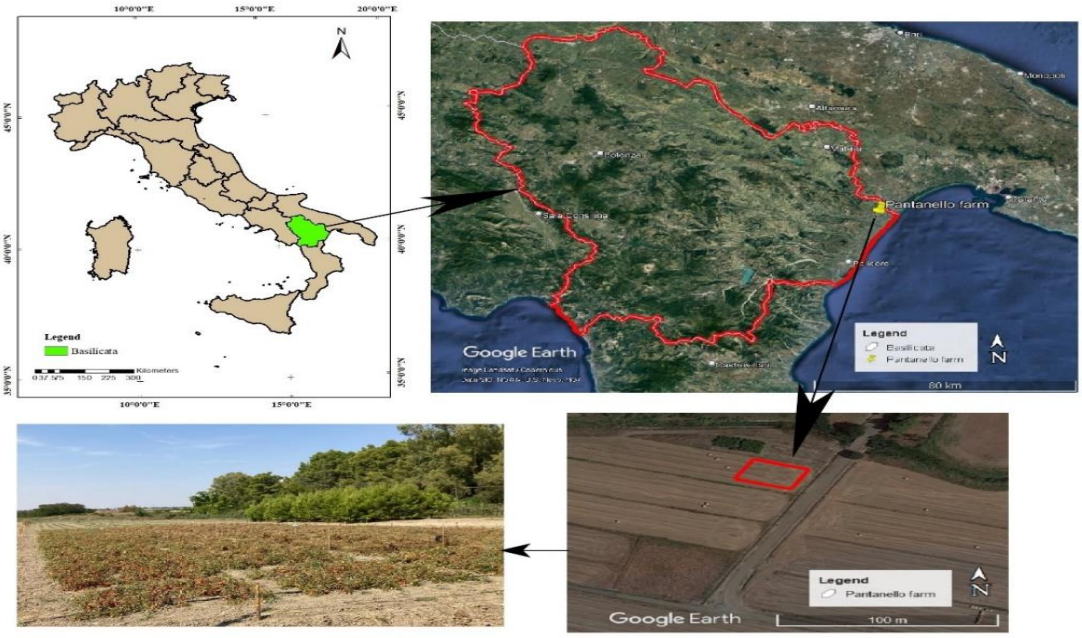

Figure 3. A schematic view of the experimental site Pantanello

As the official reported by the Basilicata Region website in 2020, the ALSIA climatic station, Metaponto farm Pantanello (25 m a.s.l.), is shown the average precipitation is between 550 mm per year. Rainfall distribution is more abundant in autumn and winter. The maximum monthly values are reached in December with 75 mm and the monthly lowest are in July and August, with 14 mm in both months. The average annual temperature is about 17 °C . The highest monthly averages are in July and August, around 26 °C, and the lowest in January around 8.1 °C.

The thermo-pluviometric data, based on the Bagnouls and Gaussen diagram, show that the period of water deficit goes from May to September. The soil moisture regime, estimated with the Billaux method, is xeric, and the temperature regime of soils is thermal.

The site is characterized by a Mediterranean climate according to the De Martonne classification (Cantore, et al., 1987). The texture of the first two soil horizons is classified as silty-clay.

2.2. experimental setup

The study was conducted on two varieties of tomato, namely *Pizzutello di Sciacca* and *Locale di Salina*. Tomatoes are the second most consumed vegetable crop worldwide (Frusciante et al., 2000; Willcox et al., 2003). It has high water demands due to the high ET_p rates (Cantero-Navarro et al., 2016) and is reported to be sensitive to water deficits (Rudich et al., 1977; Babalola and Fawusi, 1980).

The succession of operations generally involved deep plowing (30 cm) and successive land milling. The transplant took place in May 2020 using seedlings of tomato with determined growth at the third fourth true leaf stage. The row distance was 1.8 m while the distance between plants on the rows was 0.30 m, in order to obtain a density of 1.85 plants per m^2. Fertilization was done with 100-120 kg/ha of P_2O_5, 150-200 kg/ha of K_2O and 180-200 kg / ha of nitrogen.

The experimental site was subdivided into 16 plots of 18 m^2 (6m × 3m), divided into two series of 8 plots, one irrigated with full irrigation (100% of the potential evapotranspiration, ET_p) and one with

Deficit Irrigation, DI, (80% of ET_p). Both tomato varieties were cultivated in each of the two series of plots (Figure 4). This experimental scheme allowed exploring the dependence of transpiration fluxes on the variability of soil hydraulic properties also under deficit irrigation and different crop varieties. The two series of plots were arranged according to a completely randomized design.

Irrigation was applied by a dripper irrigation system. The irrigation system was carefully designed to guarantee an irrigation uniformity of more than 90%. During the whole growth season, 14 irrigations were made involving a total seasonal irrigation volume of 5.3 m^3 in control plots (100% irrigation) and 4.45 m^3 in water stressed plots (80% irrigation). The berries were harvested at the end of August 2020.

Figure 4. A schematic view of the experimental design and a picture of the field at the harvesting time. Note the crop covering the plots completely

2.3. Meteorological data

Meteorological data were needed for the simulation model. They were collected from a nearby meteorological station. These data included: temperature, humidity, wind speed, and solar net radiation, which allowed calculating the reference evapotranspiration, ET_0, by the Penman-Monteith equation, which was converted to potential evapotranspiration, ET_p, of tomato by using appropriate crop coefficients, Kc.

2.4. Measurement methods

2.4.1. Measuring soil hydraulic properties and their variability

In this study, a novel fast soil hydraulic characterization method, the **TDR-2Dmod** method, was used, which integrates time domain reflectometry TDR measurements and 2D transient modeling of the water content dynamics in the wetted bulb developing in the soil under a point-source (Coppola *et al*., 2022). In practice, the method consists of irrigating the soil by a dripper (the point-source) and monitoring the dynamics of the water content in the wetted bulb in the soil under the dripper by one or more TDR probes. Inverse 2D modeling of this dynamics allows estimating the parameters of soil hydraulic properties under the dripper by using an optimization algorithm that minimizes an objective function, including the residuals between observed and simulated water contents. To this aim, the hydraulic functions are described by using parametric equations (Russo, 1988; van Genuchten, 1980). Based on monitoring the evolution of the water bulb below a dripper, the method's strength is that it may be used for estimating the hydraulic properties in several sites simultaneously by a single field experiment involving irrigation of the field under study by a dripper system.

The method describes the dynamics of the water inside the wetted bulb by the Warrick (1974) analytical solution of Richard's equation for flow from a point source (the dripper in our case) (for details on the Warrick analytical solution, see the appendix A.1.).

The soil hydraulic parameters (α_{GR} and K_s) used for linearizing the Warrick (1974) analytical solutions were determined as follows: In each of the 16 experimental plots, a four l/h, pressure compensated dripper was used as a point source to irrigate the soil. The whole irrigation test lasted about 2 hours. The dripper, taken at 5 cm from the soil surface, was connected to a Mariotte water reservoir with a bubbling point at 1 m from the dripper. A preliminary test was carried out to know the actual dripper flow rate at a 1 m pressure head. On average, an actual flow rate of 3.7 l/h was measured and used as input for the simulations by the 2D model. During irrigation, the water content evolution in the wetting bulb was monitored by using a two-wire probe, 25 cm length, 0.6 cm rod

diameter, and 7 cm external rod spacing. The probe was provided with an adapter (balun) to connect the coaxial cable to the two rods. The balun was immersed in the head of the probe, which was 8 cm wide, 4 cm in height, and 1.5 cm in thickness. The probe was embedded vertically below the dripper. To avoid interference with the dripping, the probe was installed with a very small insertion angle as shown in (Figure 6.b) During the infiltration experiment, the waveform was acquired at 2 minutes intervals by using a time domain reflectometry (TDR100) device (Campbell Scientific). Acquisition and subsequent interpretation of the TDR waveforms were performed utilizing the specifically developed software. Before installation, the laboratory calibrated probes for water content measurements. The layout of the experimental setup is depicted in Figure 5.

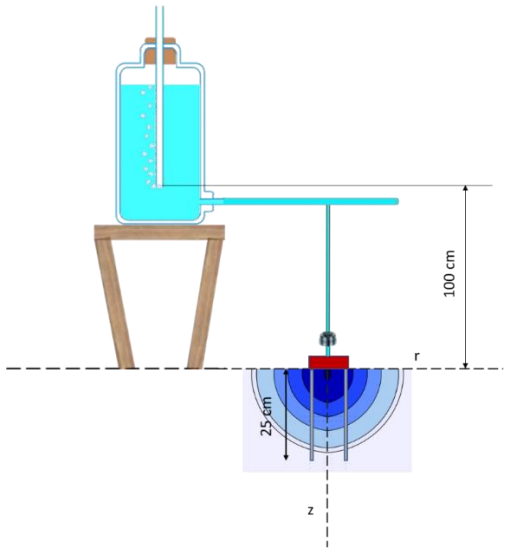

Figure 5. Experimental setup used for hydraulic characterization by the TDR-2Dmod method (not to scale)

All the data about the actual flow rate and the water contents measured by the TDR probe were used as input for a 2D modeling of the water distribution and dynamics in the wetted bulb based on the Warrick analytical solution for 2D flow from a point source. An inversion algorithm was aimed at minimizing the differences between the water contents measured by the TDR probe (hereafter θ_{TDR}) and the average water content predicted by the 2D model (hereafter θ_{2D}) in the same soil volume explored by the TDR probe allowed for optimizing the parameters of the hydraulic properties in each

of the irrigated sites. Appendix A provides details on the water content calculation in the wetted bulb below a dripper by using the Warrick (1974) analytical solution for 2D flow from a point source.

The parameters α_{GRD}, k, and K_s were considered as fitting parameters. The parameters were estimated by solving an optimization problem that minimizes the deviations between the water content measured by the TDR probe (precisely, the average water content in the volume sampled by the TDR probe) and the average water content obtained by the 2D simulation in an observation volume comparable to that of TDR probe. The problem to be solved entails identifying the vector **b** of the fitting parameters that minimize the following objective function:

$$O(\boldsymbol{b}) = \sum_{i=1}^{N} [\theta_{TDR}(t_i) - \theta_{2D}(t_i.\boldsymbol{b})]^2 \qquad (4)$$

It involves the deviations between measured and simulated water contents at specified times t_i (i=1, 2,..N). Determination of **b** was obtained by starting from an initial estimate of parameters $\mathbf{b_i}$, using the optimization algorithm of Levenberg-Marquardt. The method also supplies information on the uncertainty of estimated parameters, evaluating a first order approximation of the covariance matrix of the parameters and calculating the confidence intervals of the individual parameters.

Crucial for the comparison is the appropriate evaluation of the volumes involved in the water content measurement by TDR and that obtained by the 2D simulation of the flow field in the soil below the dripper. According to Topp and Ferré (2002), based on the calculations of the electrical field around the rods of a TDR probe proposed by Knight *et al*. (1994), θ_{TDR} refers to an observation volume of the TDR probe which may be approximated by that of a cylinder of length equal to the length of the TDR rods (25 cm) and a diameter of about 1.5 times the outer rod spacing (10.5 cm). Thus, the volume explored by the TDR probe used in this study is approximately 2160 cm^3. To make measurement and simulated volumes actually comparable, θ_{2D} was obtained by averaging the simulated water contents in all the simulation nodes included in the volume explored by TDR. This may be seen in Figure 6, showing the simulation nodes (cross symbols) in a vertical section of the wetted bulb included in half

of the TDR observation window (about 7 cm wide). Because of the radial symmetry of the simulated water content in the bulb, the water contents simulated on one half of the bulb are exactly the same in the other half. The same may be imagined for all the radial directions other than that shown in the figure. Thus, the average water content obtained in the planar window (half TDR section) shown in the figure exactly corresponds to the average water content in the whole volume explored by the probe. Note in the figure that the calculation of the simulated average water content also includes a band of nodes a bit out of the TDR physical edge, to account for the fact that the TDR probe explores a lateral size higher than the rods distance (about 1.5 times this distance). In other words, the average simulated water content was calculated on all the simulation nodes included in an area of 25 cm × 5.25 cm. As the simulation was carried out by discretizing the flow field in both depth and radial increments of 1 cm, the window considered for calculating the average simulated water content included six horizontal compartments and 25 vertical compartments for a total of 150 (25 × 6) nodes included in the calculation (excluding the nodes at r = 0 and z = 0).

Based on the procedure described above, the inversion forces the 2D model to provide water content (and pressure heads) in the TDR observation window comparable to those measured by TDR.

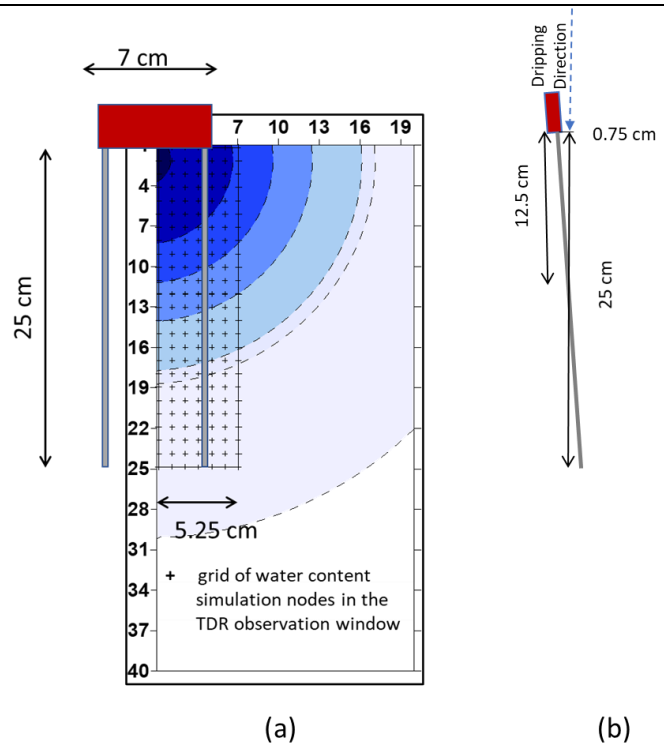

Figure 6. a) Schematic view of the portion of the 2D simulated flow field below the dripper used to calculate the average simulated water content to be compared to the measured one. The darker color in the wetted bulb indicates higher water contents; b) lateral view of the TDR probe showing the small insertion angle to avoid interference with dripping

2.4.2. Measuring crop parameters

2.4.2.1. Measuring Stomatal conductance, transpiration, and photosynthesis at the leaf scale

Field measurements of stomatal conductance, transpiration, and photosynthesis were carried out using the CIRAS-3 system (PP Systems, 2017). CIRAS-3 refers to a combined infrared analysis system. The system pumps and samples fresh air into infrared gas analyzers, IRGAs. Figure 7 shows a schematic view of the IRGA system. Each IRGA consists of an infrared source, a sample cell of known volume and length, an optical interference filter and an infrared detector.

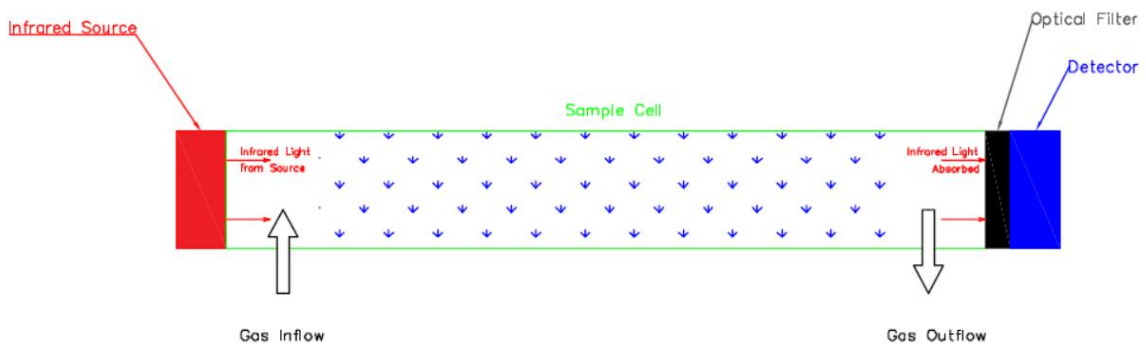

Figure 7. Schematic view of the IRGA system adopted from PP Systems (2017). Each IRGA consists of an infrared source, a sample cell of known volume and length, an optical interference filter and an infrared detector.

The infrared source produces light with mid-infrared wavelengths. The optical interference filter narrows down the light bandwidth (i.e., the range of light frequencies) to the signature wavelength, which is absorbed by gas molecules of interest (i.e., CO_2 or H_2O). When the gas fills the sample cells, it absorbs the infrared light, IR, and the IR detector measures the reduction in IR strength is measured by the IR detector. This reduction can be translated into the concentration of the gas of interest according to Beer's law. Thus, the concentration of CO_2 and H_2O can be measured using CIRAS-3 electronic processors by detecting the absorption of IR at the wavelengths 4.26 µm and 2.6 µm, respectively.

The flowmeter in CIRAS-3 measures the air volume flow rate (V_0) in cm^3/min at standard temperature and pressure conditions (STP), i.e., at 0^o C and 1013.25 mb. The ideal gas molar volume is 22.141 L/mol in STP. Therefore, the mass flow of air (W) entering the cuvette in mol m^{-2} s^{-1} is:

$$W = \left(\frac{V_0}{60 \times 1000}\right) \times \left(\frac{1}{22.414}\right) \times \left(\frac{10^4}{a}\right) \quad (5)$$

Where a is the projected leaf area in cm^2, the numbers in the equations are for unit conversions.

The transpiration rate can be calculated from the partial pressures of water vapor entering (e_{in}) and exiting (e_{out}) the cuvette. The water vapor's molar flow rate into the cuvette in mol m^2 s^{-1} is:

$$W_{vapor,in} = W \times \left(\frac{e_{in}}{P}\right) \quad (6)$$

Where P is the atmospheric pressure.

The air flow out of the cuvette is increased by the transpiration rate, T. Thus, the molar flow of water vapor out of the cuvette is:

$$W_{vapor,out} = (W + T) \times \left(\frac{e_{out}}{P}\right) \quad (7)$$

Therefore, the transpiration rate in mol m^{-2} s^{-1} is the difference between the molar air flow into and out of the cuvette:

$$T = \left[(W + T) \times \left(\frac{e_{out}}{P}\right)\right] - \left[W \times \left(\frac{e_{in}}{P}\right)\right]$$
$$T = \left[\frac{W \times (e_{out} - e_{in})}{(P - e_{out})}\right] \quad (8)$$

The difference between leaf and air temperatures, Dt, can be calculated as (Parkinson, 1983):

$$\Delta t = \left[\frac{H - \lambda \times T}{\left(\frac{0.93 \times M_a \times C_p}{r_b}\right) + [4\sigma \times (t_c + 273)^3]}\right] \quad (9)$$

Where H is the radiation absorbed by the leaf, λ is the latent heat by vaporization of water, T is the transpiration rate, M_a is the air molecular weight, C_p is the specific heat at constant pressure, r_b is the boundary layer resistance to vapor transfer which is empirically determined for each cuvette using a filter paper, σ is the Stefan Boltzmann constant and t_c is the cuvette temperature.

The leaf temperature can then be calculated as:

$$t_{leaf} = t_c + \Delta t \quad (10)$$

The saturation vapor pressure, e_{leaf} can be calculated from t_{leaf} (Buck, 1981):

$$e_{leaf} = 6.1365 \times \exp\left(\frac{17.502 t_{leaf}}{240.97 + t_{leaf}}\right) \quad (11)$$

The total conductance, g_{total}, can be calculated using von Caemmerer and Farquhar (1981) model:

$$g_{total} = \frac{T \times \left(P - \frac{e_{leaf} + e_{out}}{2}\right)}{(e_{leaf} - e_{out})} \quad (12)$$

However, the total conductance is $[1/(r_s+r_b)]$ where r_s is the stomatal resistance and r_b is the boundary resistance. Therefore, the stomatal resistance, r_s in m^2 s mol^{-1} is:

$$r_s = \left[\frac{e_{leaf} - e_{out}}{T \times \left(P - \frac{e_{leaf} + e_{out}}{2}\right)}\right] - r_b \quad (13)$$

And then the stomatal conductance g_s can be calculated as $(1/ r_s)$.

The net photosynthesis, A, can be calculated from the difference between CO_2 concentrations entering (C_{in}) and exiting (C_{out}) the cuvette. The CO_2 readings by IRGA are corrected for vapor pressure, temperature and atmospheric pressure. The additional vapor from transpiration dilutes the C_{out} concentration. Thus, it is compensated as follows:

$$A = (C_{in} \times W) - C_{out} \times (W + T) \quad (14)$$

2.4.2.2. Leaf Area Index, LAI, and crop coefficient, K_c

Agro-hydrological simulations require the vegetation parameters, namely the Leaf-Area Index, LAI, and the crop coefficient, K_c. LAI is defined as the total leaf area to the total ground area. LAI is necessary because it partitions the evapotranspiration between soil evaporation and plant transpiration. The crop coefficient is also necessary to obtain the tomato potential evapotranspiration, ET_p, from the reference evapotranspiration, ET_0.

For this purpose, LAI was measured in the field using the leaf area meter (LI-3000, with conveyor belt assembly, LI-3050; Li-Cor, inc., Lincoln, NE, USA) on 19 May, 4 June, 19 June, 8 July, 6 August

and 10 August 2020 for all 16 plots. The daily values of LAI during the growth season were then obtained by the interpolation of the six measurements.

Crop coefficient, K_c, values were obtained from the literature as a function of the LAI by the equation proposed by Čereković et al. (2010) for tomato fields in southern Italy:

$$K_c = 0.2018 \ln(LAI) + 1.0926 \quad (3)$$

The reference evapotranspiration, ET_0, was obtained using the Penman-Monteith equation utilizing the meteorological data. Coefficient K_c was then used to obtain the crop potential evapotranspiration, Etc, as (K_c ET_0).

2.5. Simulation model

The Agro-hydrological model utilized in this thesis is FLOWS-HAGES model (Coppola *et al.*, 2019). This model simulates the vertical transient flow in vegetated soils using the one-dimensional Richards equation (equation (4)). The equation is solved using implicit finite differences with explicit linearization similar to SWAP model (Van Dam *et al.*, 1997).

$$C(h)\frac{\partial h}{\partial t} = \frac{\partial}{\partial z}\left(K(h)\frac{\partial h}{\partial z} - K(h)\right) - S_w(h) \quad (4)$$

where C(h)=dθ/dh (L^{-1}) is the soil water capacity, h (L) is the soil water pressure head, t (T) is time, z (L) is the vertical coordinate being positive upward, K(h) (L T^{-1}) is the hydraulic conductivity and S_w(h) (T^{-1}) is a sink term describing water uptake by plant roots.

Equation (4) requires the soil hydraulic parameters, i.e., water retention and hydraulic conductivity parameters. In this study, the water retention properties were described as (van Genuchten, 1980):

$$\begin{aligned} S_e = \frac{\theta - \theta_r}{\theta_s - \theta_r} = [1 + |\alpha_{VG} h|^n]^{-m} \quad & h < 0 \\ \theta = \theta_s \quad & h = 0 \end{aligned} \quad (5)$$

where S_e is the effective saturation, h is the soil water potential, θ is the soil water content, θ_s is the water content at saturation and θ_r is the residual water content. α_{VG} [cm^{-1}], n and m = 1-1/n are shape parameters. This water retention model was applied to Mualem's model as to obtain the relative hydraulic conductivity, $K_r(S_e)$:

$$K_r(S_e) = \frac{K(S_e)}{K_0} = S_e^{\tau}\left[1 - \left(1 - S_e^{1/m}\right)^m\right]^2 \quad (6)$$

where K_r is the relative hydraulic conductivity, K_0 is the saturated hydraulic conductivity and τ is a parameter to account for tortuosity.

Root-water uptake was calculated using Feddes-type macroscopic approach that calculates the actual sink term in equation (4) empirically using observed responses to water and osmotic potentials (Feddes, 1978, 2004). This study focuses on the water stress, and thus, the sink term in equation (4) becomes $S_a(h)$ which depends on: 1) the root density distribution function g(z), and 2) the activity at any depth in the root zone during the crop's growth season. A uniform root density distribution function was adopted (Feddes, 1978):

$$g(z) = \frac{1}{Dr} \quad (7)$$

where Dr is the root depth.

The potential root water uptake over the unit depth at any depth along the root zone, S_p (T^{-1}), was calculated by distributing the potential transpiration, T_p (L T^{-1}), over the root zone depth, Dr (L), in proportion to the root density distribution, g(z) (Feddes, 1978; Feddes and Raats, 2004):

$$S_p(z) = g(z)T_p \quad (8)$$

Low water availability, i.e., water stress, reduces the potential root water uptake. The reduction coefficient, α_{rw}, is thus introduced to obtain the actual sink term under water stress (Feddes, 1978):

$$S_a = \alpha_{rw}(h)S_p = \alpha_{rw}(h)g(z)T_p \quad (9)$$

The reduction coefficient, α_{rw}, follows a linear relationship with the soil-water pressure head, *h*, as shown in Figure 8. The optimal conditions with no reduction in root water uptake occur when the stress occur when h is between h_2 and h_3. Reduction in root water uptake can occur when *h* falls below h_3 (water deficit) or when it is higher than h_2 (oxygen deficit).

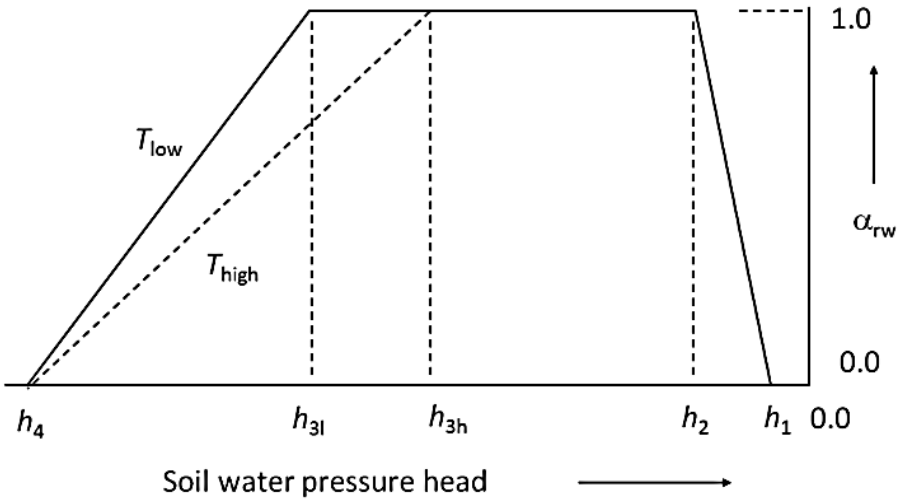

Figure 8. The relationship between the soil-water pressure head, *h*, and Feddes reduction coefficient, α_{rw}. Stress occurs when the pressure head falls below h_3 (water deficit) or when it is higher than h_2 (oxygen deficit).

The potential transpiration itself, T_p, is obtained from the potential evapotranspiration, ET_p, using the Leaf-Area Index, LAI, and an extinction factor, *k*, to account for solar radiation attenuation:

$$T_p = \mathrm{ET_p} \times \frac{1 - \exp(-k \times LAI)}{k} \quad (10)$$

FLOWS requires the following input data to carry out the simulations:

1. Soil hydraulic properties, i.e., soil-water retention and hydraulic conductivity,
2. Vegetation parameters, i.e., LAI and K_c;
3. Reference evapotranspiration, ET_0;

4. Irrigation management parameters (in case the irrigation fluxes are computed by the model), namely the critical pressure head value, h_c, and the critical depth, z_c; and
5. Irrigation fluxes (in case of analyzing registered irrigation data as an input)

FLOWS simulation output, thus, provides information on the daily evolution of the following:

1. soil-water pressure head,
2. soil-water content,
3. soil-water fluxes, and
4. irrigation fluxes computed by the model

As for the irrigation settings in FLOWS, there are two configurations: 1) irrigation given by the user and 2) irrigation computed by the model. In the first configuration, daily irrigation fluxes are introduced to the model as input by the user. In this case, the simulations mainly aim at analyzing the current situation or registered irrigation practices. In the second configuration, the irrigation fluxes are optimized by FLOWS according to the criteria shown in Figure *9*. There are two parameters set by the user in case of irrigation computed by the model: h_c and z_c. The model calculates the average pressure head along z_c, h_{av}, and if it is lower than the critical value, h_c, then irrigation begins with the objective of bringing h_{av} to the field capacity, h_{fc}. In this study, the irrigation volumes were introduced as an input, i.e., using the first configuration (irrigation given by user).

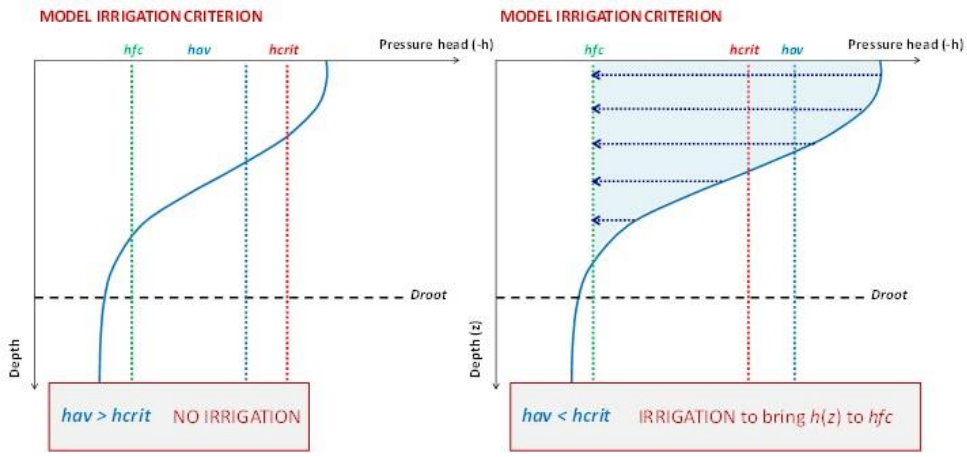

Figure 9. Graphical view of the on which the model is based to compute the time and volume of irrigation. (a) h_{av} higher than h_c, no irrigation is required; (b) h_{av} lower than h_c, irrigation is required to bring the pressure head at the field capacity, h_{fc}.

Figure 10 shows the interface of FLOWS model. FLOWS interface is user friendly with separate windows to include all the input data necessary for Agro-hydrological simulations. Figure 11 shows the recommended order of inputs to be given by the user to carry out the simulations.

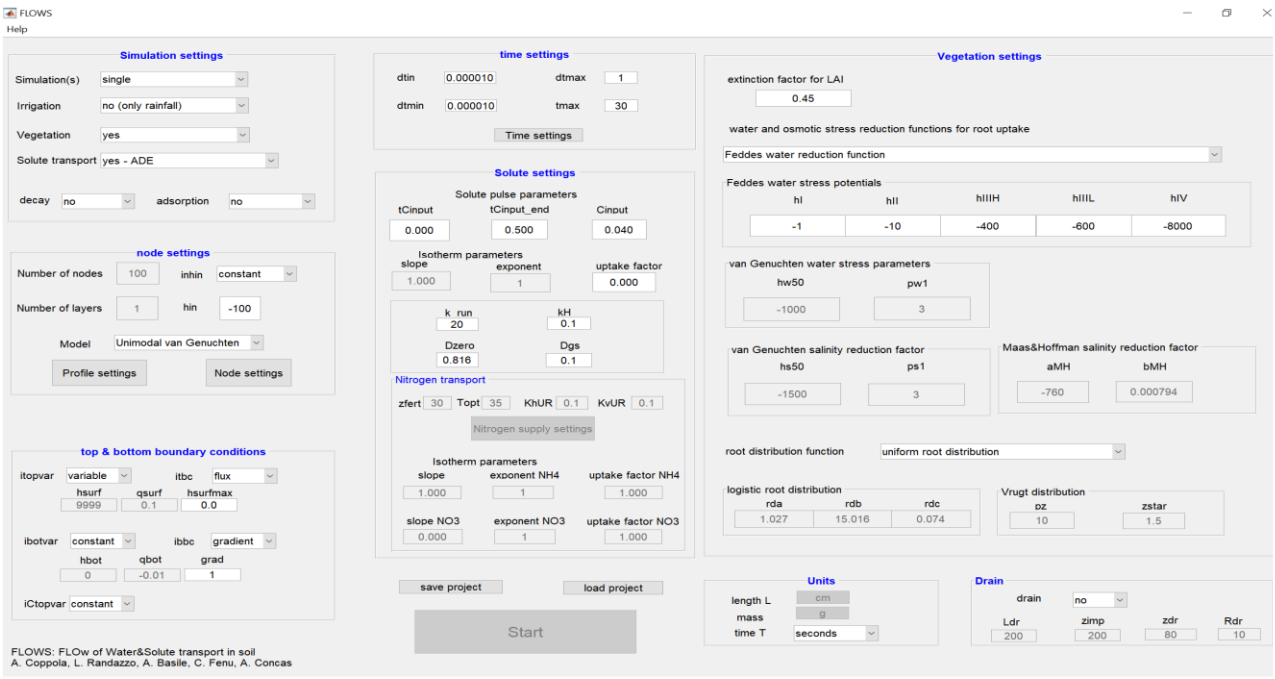

Figure 10. FLOWS model interface with all the input windows

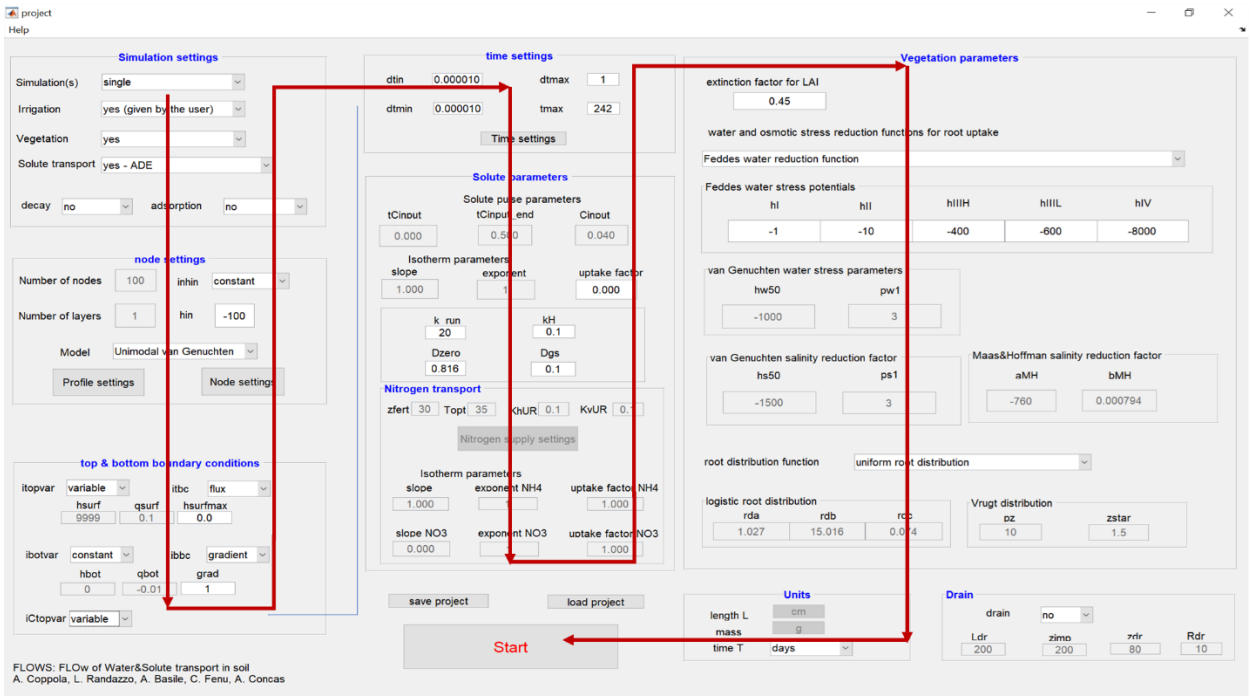

Figure 11. FLOWS model interface. The red arrows represent the recommended flow of input data to be provided by the user to carry out the Agro-hydrological simulations.

The most important datasets for FLOWS model are:

1. The simulation settings: the irrigation configuration (i.e., given by the user or computed by FLOWS) and the solute transport settings (if needed);
2. The profile settings: the soil hydraulic properties of different soil layers and the number of nodes for the finite-difference solution; and
3. The time settings: the daily evolution of the vegetation parameters (i.e., LAI and K_c), the reference evapotranspiration and the root depth

Chapter 3

3. Results and Discussion

The following chapter displays the results from both the field study as well as the computer simulations. The results from the field and laboratory were used as inputs in Flows-Hages Model.

3.1. Soil hydraulic properties and their variability (tables, maps, etc)

Table *1* reports the soil hydraulic property parameters in the 16 plots, as well as the averages and the standard deviations of those parameters. The results show that plot R1-4 had a particularly low saturated hydraulic conductivity, K_s, with a value of 18.974 cm/d; in contrast, plot R1-3 had the highest K_s value, with 293 cm/d among the plots.

Table 1. The soil hydraulic parameter values for all 16 plots, as well as their averages and standard deviations

Plot	r_b (g m^{-3})	q_s (m^3m^{-3})	α	*n*	K_s (cm/day)
R1-1	1.364	0.485	0.034	2.579	111.348
R1-2	1.267	0.522	0.009	2.259	121.812
R1-3	1.314	0.504	0.010	2.116	293.558
R1-4	1.248	0.529	0.013	2.366	18.974
R1-5	1.364	0.485	0.013	2.539	78.111
R1-6	1.267	0.522	0.016	2.651	104.349
R1-7	1.314	0.504	0.039	2.190	111.480
R1-8	1.248	0.529	0.013	2.506	48.682
R2-1	1.364	0.485	0.011	2.437	143.994
R2-2	1.267	0.522	0.016	2.472	84.550
R2-3	1.314	0.504	0.012	2.226	87.879
R2-4	1.248	0.529	0.036	2.295	142.719
R2-5	1.364	0.485	0.016	2.616	74.020
R2-6	1.267	0.522	0.014	2.157	69.570
R2-7	1.248	0.529	0.012	2.330	40.364
R2-8	1.314	0.504	0.015	2.403	66.414
Average	1.299	0.510	0.017	2.384	99.864
Standard Deviation	0.046	0.017	0.010	0.168	62.359

Soil hydraulic properties were used to generate maps to show the resulting distribution of the Van Genuchten parameters. Figure *12* shows the hydraulic parameters of all 16 plots in the study area as color-graduated maps, including saturated water content, θ_s , the parameter α_{vG} , the parameter n_{vG}, and the saturated hydraulic conductivity, K_s in the field measurements.

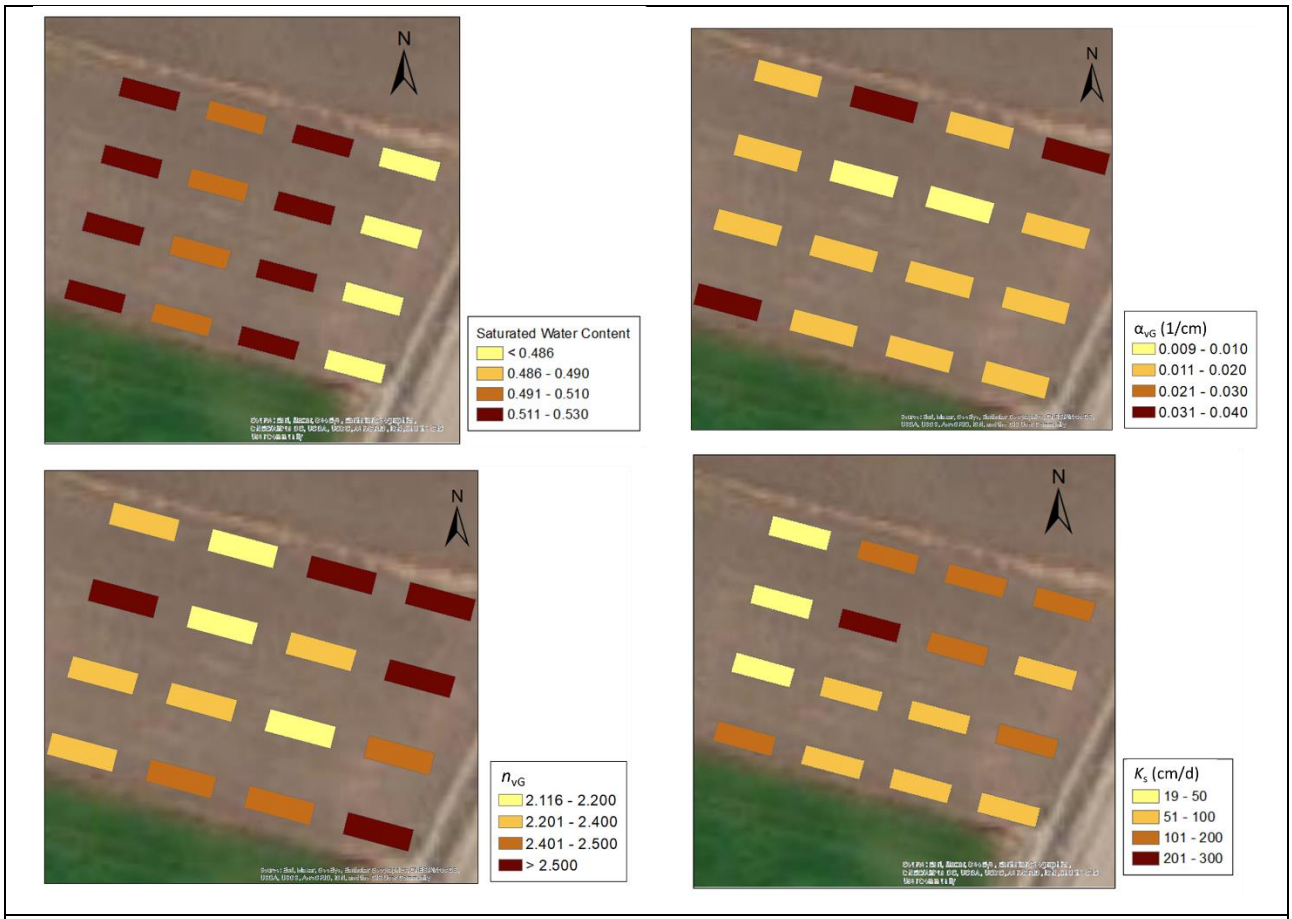

Figure 12. Color-graduated maps of the hydraulic property parameters. Clockwise from upper left: saturated water contents, θ_s, van Genuchten parameter α_{vG}, the saturated hydraulic conductivity, K_s, and the van Genuchten parameter n_{vG}

Table 1 and figure 12 show that the spatial variability of soil hydraulic parameters in the study area is especially apparent for the saturated hydraulic conductivity. In any case, the parameter α_{vG} varies between 0.009 and 0.03, which may have important effects on the simulations for high water contents. The parameter n_{vG} has an average value of 2.384 (table 1). This latter finding was not expected in the silty-clay soil in the study area. However, this can be explained by the soil structure; the soil is well-

structured. This can be also found in the high values of Ks. In any case, the hydraulic properties were found to be spatially variable although the study area is small.

3.1.1.Soil Water Retention Curves (SWRC)

The Soil Water Retention Curves (SWRC) are based on the soil moisture content and TDR probes gained as the average water content at each soil water pressure from the field measurements (Figure 13).

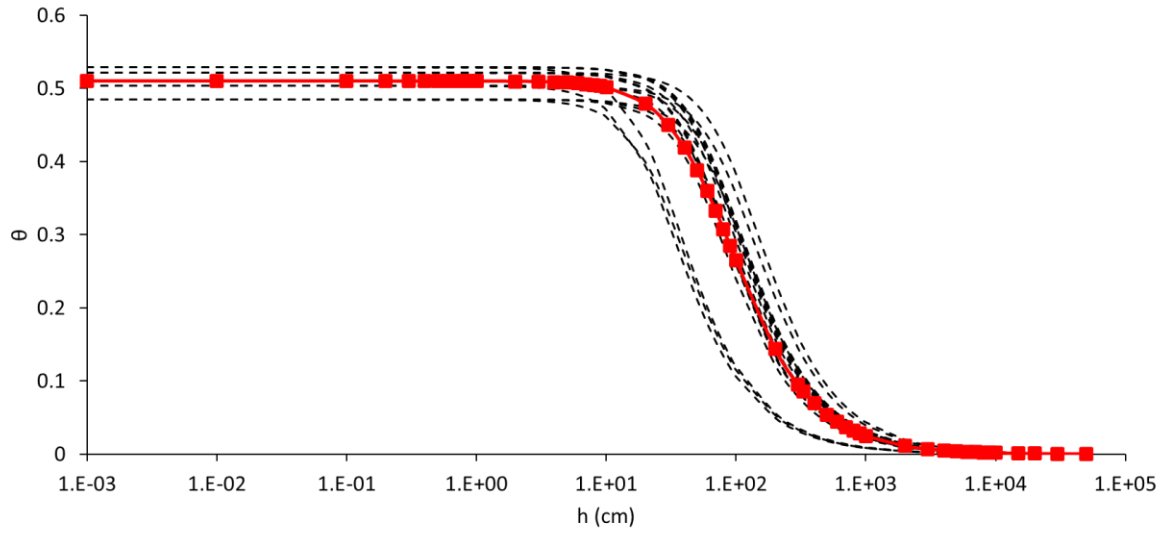

Figure 13. The Water Retention Curves, WRC, of all 16 plots (black dashed lines) as well as the average WRC obtained as the average water content at each soil water pressure (red solid lines with markers)

3.1.2. Hydraulic Conductivity Curves (HCC)

The Hydraulic Conductivity Curves (HCC) of all 16 plots and the average HCC obtained as the average hydraulic conductivity at each soil water pressure (Figure 14).

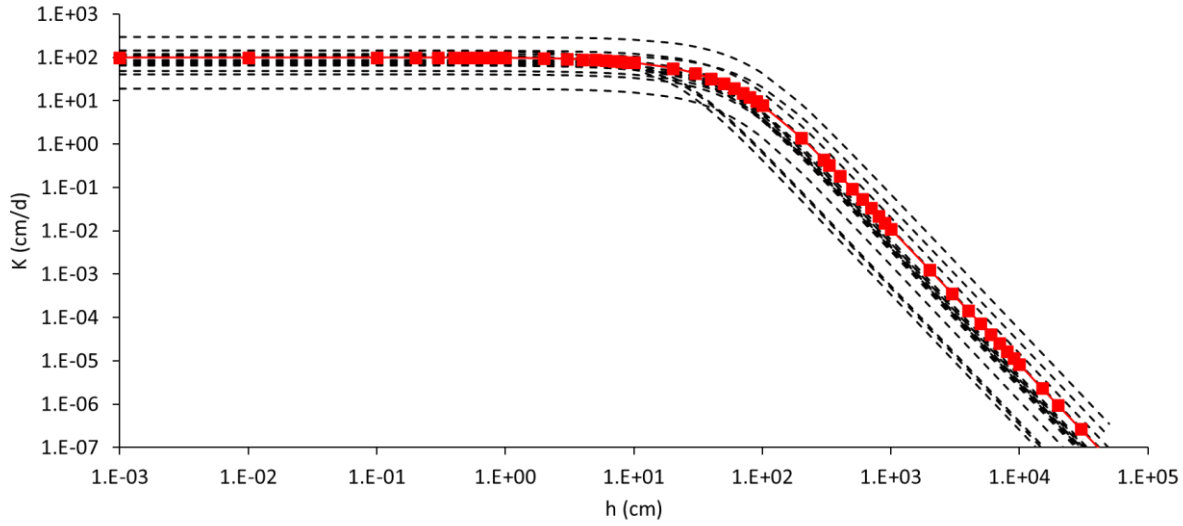

Figure 14. The Hydraulic Conductivity Curves, HCC, of all 16 plots (black dashed lines) as well as the average HCC obtained as the average hydraulic conductivity at each soil water pressure (red solid lines with markers)

3.2. Crop parameters and their variabilities

3.2.1. The leaf area index (LAI)

The Leaf-Area Indices, LAI, is an important parameter correlated directly to crop production. This study showed LAI varied between a maximum of 2.41 and a minimum of 0.65 in control plots and a maximum of 2.15 and a minimum of 0.65 in water deficit plots (Figure 15). Figure 15 shows the LAI values obtained from the field measurements for the control plots (blue line) and the plots with deficit irrigation (orange line). LAI was measured in-situ using the leaf-area meter for six days during the tomato growing season. The figure shows the lower LAI values for the deficit irrigation group, especially at the peak values.

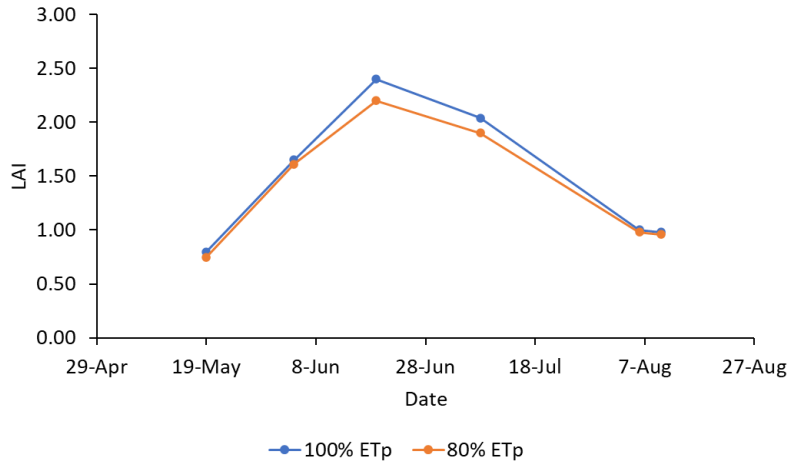

Figure 15. Leaf-Area Index, LAI, values were obtained from the field measurements for the control plots (blue line) and the plots with deficit irrigation (orange line).

3.2.2. Crop coefficient (K_c)

Crop coefficient, K_c, values for tomatoes grown are shown in Figure 16. K_c values for the initial, mid, and late-season growth stages were 0.9–1.4, 1.6–1.7, and 1.2–0.9 in control plots, respectively, and 0.8–1.4, 1.5–1.6, and 1.1–0.9 in water deficit plots, respectively.

Figure 16 shows the crop coefficient, K_c, values obtained from the Leaf-Area Index, LAI, using Čereković *et al.* (2010) proposed equation for the control plots (blue line) and the plots with deficit irrigation (orange line). Similar to LAI, K_c values were lower in the deficit irrigation group than those of the control group which was expected as the K_c values were obtained from LAI.

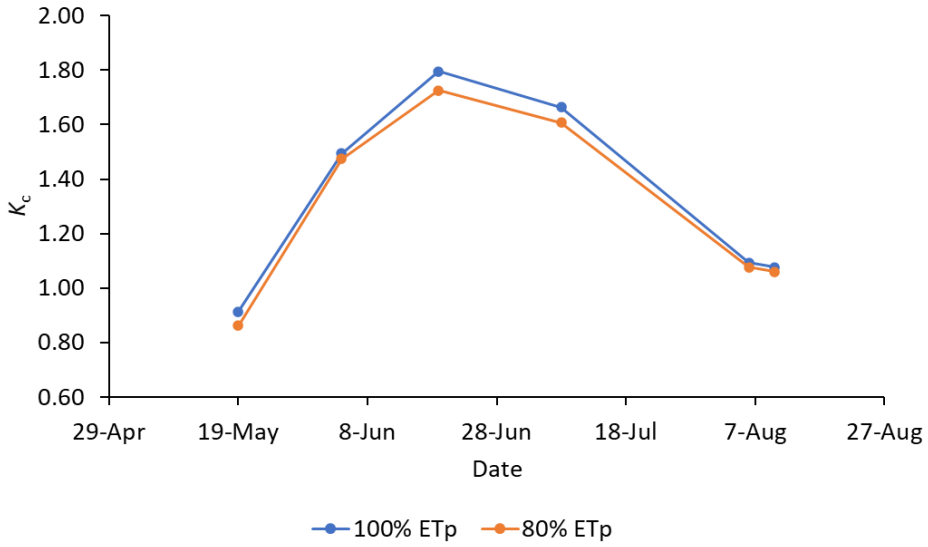

Figure 16. Crop coefficient, K_c, values obtained from the Leaf-Area Index, LAI, using Čereković *et al.* (2010) proposed equation for the control plots (blue line) and the plots with deficit irrigation (orange line).

3.2.3. canopy-scale stomatal conductance ($g_{s,c}$)

The map of canopy-scale stomatal conductance, $g_{s,c}$, illustrates in mmol/m^2 s for all 16 plots as a color-graduated map in Figure 17. The results demonstrated $g_{s,c}$ rate varied between 30 to 120 in control plots and 30 to 100 in water deficit plots.

Canopy-scale stomatal conductance was obtained by upscaling the field-measured leaf-scale stomatal conductance, $g_{s,l}$, using the big-leaf approach. The leaf-scale measurements were carried out twice on 5 and 10 August 2020, and therefore, $g_{s,c}$ values shown in the figure are the averages of the two measurements taken on the two days. The figure shows that the average canopy-scale stomatal conductance for the control group is higher than that of the deficit irrigation. In addition, the overall spatial variability of $g_{s,c}$ is high due to the high spatial variability of the leaf-scale stomatal conductance.

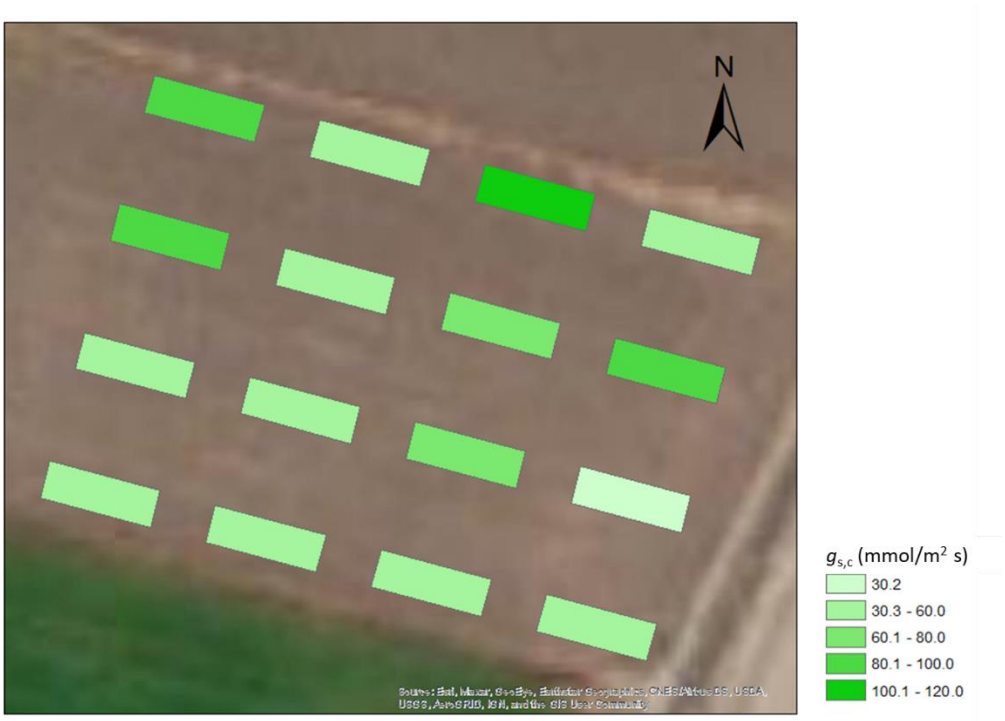

Figure 17. The canopy-scale stomatal conductance, $g_{s,c}$, in mmol/m^2 s for all 16 plots as a color-graduated map

3.2.4. Transpiration rates

The color-graduated maps of the canopy transpiration rates, $T_{a,c}$, obtained as upscaled leaf-scale transpiration rates, $T_{a,l}$, and the macroscopic transpiration rates, $T_{a,m}$, calculated by the Agro-hydrological model FLOWS-HAGES are provided in Figure 18 which $T_{a,c}$ represents the average of two measurements carried out on 5 and 10 August 2020, and $T_{a,m}$ were obtained as averages of daily transpiration rates simulated between 5 and 10 August 2020. Figure 18 indicates that the canopy transpiration rates were significantly more spatially variable than the macroscopic approach using FLOWS-HAGES Agro-hydrological model.

Figure 18. Color-graduated maps of the canopy transpiration rates, $T_{a,c}$, obtained as upscaled leaf-scale transpiration on the left and of the macroscopic transpiration rates obtained from FLOWS-HAGES model, $T_{a,m}$, on the right.

As for the $T_{a,l}$ and $T_{a,c}$, the R1 transpiration rates are on average higher than the R2 plots, but with a much larger variability, such that in some cases the R1 transpiration rate is either similar or even lower than that observed in the R2 plots. The $T_{a,m}$ values confirm the average behavior observed in the $T_{a,l}$ and $T_{a,c}$ cases. Only in one case (plot R1-4), the transpiration rate simulated for the 100% irrigation volume produces a stress similar to that simulated for the 80% irrigation volume.

3.3. Simulation results

Figure 19 shows the daily cumulative actual transpiration rates obtained using the macroscopic approach, $T_{a,m}$, for all 16 plots in the study area. Also, The daily ratios between the cumulative actual transpiration rates obtained using the macroscopic approach, $T_{a,m}$, and the cumulative potential transpiration rates, T_p, in all 16 plots are shown in Figure 20.

Figure 19 shows that, although R1 plots had generally higher $T_{a,m}$ rates than those of the R2 group, plot R1-4 had particularly lower $T_{a,m}$ rates than the rest of R1 group. Plot R1-4 experienced water stress although it was supplied with 100% of ET_p.

Looking at Figure 20, it is observed that, generally, the R1 group's ratio of cumulative ($T_{a,m}$ / T_p) was close to 1.00 except for plot R1-4 whose ratio was below 0.8 similar to R2 group. However, the water stress in plot R1-4 stems from the hydrological, soil-water, processes; the water stress, in this case, was a direct result of the soil hydraulic properties rather than the quantity of applied irrigation water. More information about the relationship between the transpiration rates obtained by the macroscopic approach and the soil hydraulic properties are shown in section (3.5.2. Relationship between transpiration rates obtained by FLOWS-HAGES, the soil hydraulic parameters and the canopy-scale stomatal conductance).

Using the Agro-hydrological model to obtain the root water uptake, and subsequently, the transpiration rates (i.e., the macroscopic approach), provided sufficient information about the temporal variability of transpiration rates along all growth seasons as shown in Figure 19 and Figure 20. This information, on the other hand, is more complicated to obtain using the microscopic approach as it requires extensive field measurements rather than using mathematical models.

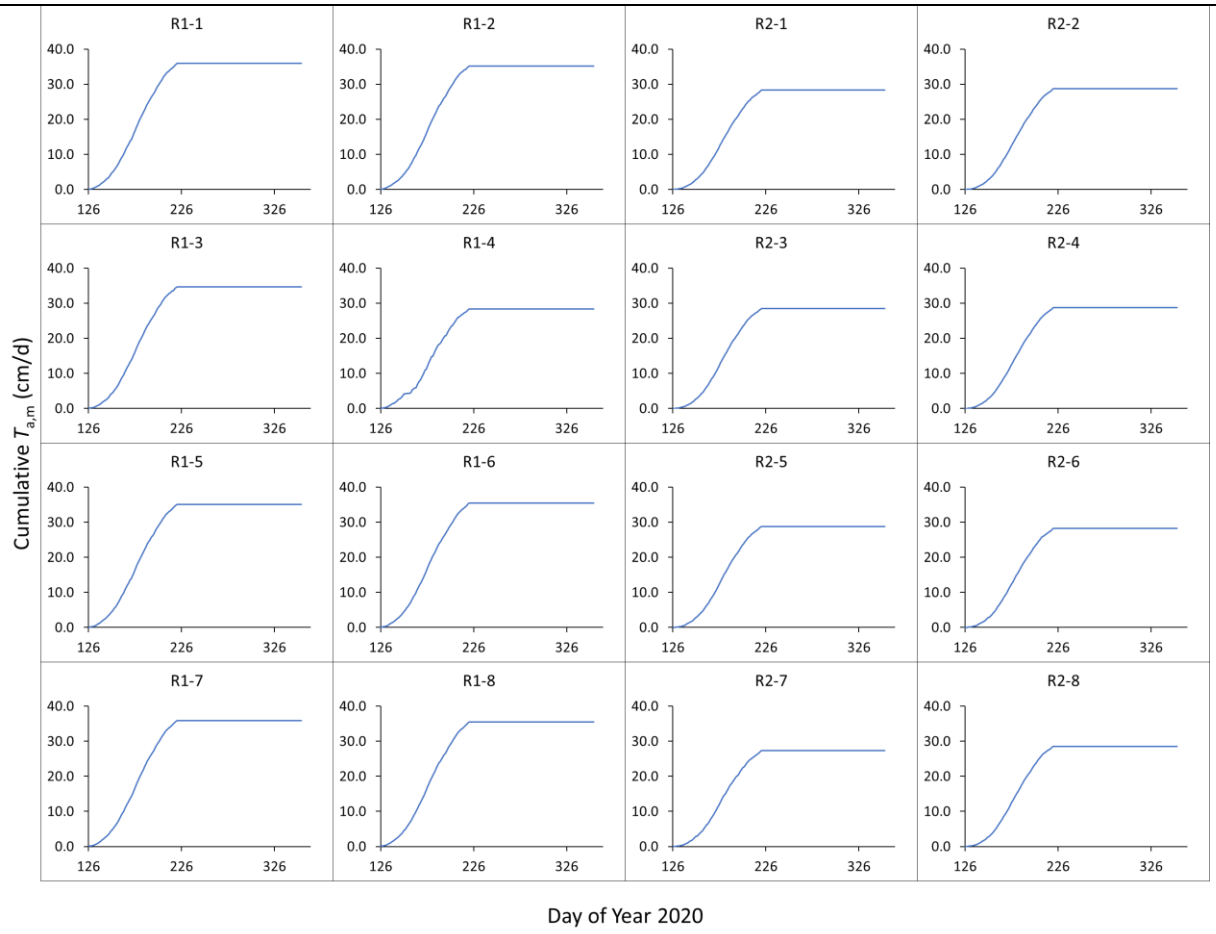

Figure 19. The daily cumulative actual transpiration rates obtained using the macroscopic approach, $T_{a,m}$, for all 16 plots in the study area

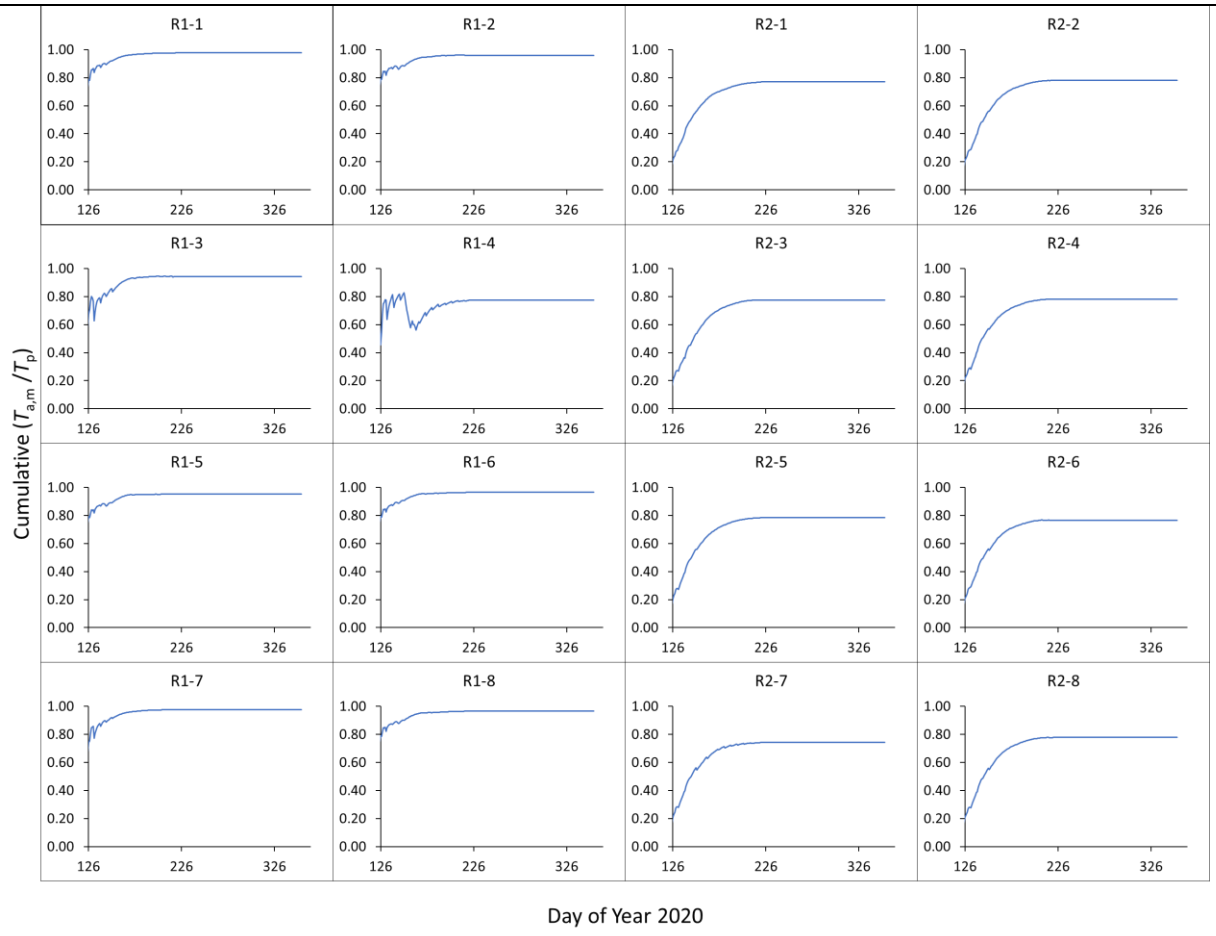

Figure 20. The daily ratio between cumulative actual transpiration rates obtained using the macroscopic approach, $T_{a,m}$, and the cumulative potential transpiration rates, T_p, for all 16 plots in the study area

3.4. Comparing simulated and measured root uptake (transpiration rates in the canopy scale, and the macroscopic)

Figure 21 shows the canopy-scale transpiration rates, $T_{a,c}$, (blue line), the leaf-scale transpiration rates, $T_{a,l}$, (black line) and the macroscopic transpiration rates calculated by FLOWS-HAGES, $T_{a,m}$, Agro-hydrological model (orange line) for all 16 plots. Plots names starting with R1 refer to the control plots while those starting with R2 refer to the plots with deficit irrigation. The mean values for $T_{a,c}$ and $T_{a,m}$ were 0.46 and 0.38 cm/day, respectively, while the standard deviations were 0.09 and 0.17 cm/day, respectively. The lower variability of the $T_{a,m}$ indicates that the agro-hydrological model

smooths the transpiration rate variability in a way similar to Fourier's transformation by filtering out the high-frequency variability. The transpiration rates obtained from the Agro-hydrological model are more useful from a management perspective as the model removes the erratic values coming from the high variability of the small, leaf-, scale measurements which can introduce high uncertainty levels in the transpiration evaluation at the field scale.

As for transpiration rates obtained from field measurements, i.e., $T_{a,l}$ and $T_{a,c}$, the average value for R1 group was higher than that of the R2 group. However, the variability of both $T_{a,l}$ and $T_{a,c}$ was high that in some cases the transpiration rates for R1 were similar or even smaller than those observed in R2 group. Similarly, $T_{a,m}$ values confirm the average behavior of the $T_{a,l}$ and $T_{a,c}$ except in one case (plot R1-4) which was supplied with 100% of ET_p where the simulated transpiration experienced a stress level similar to the R2 group which was supplied with 80% ET_p.

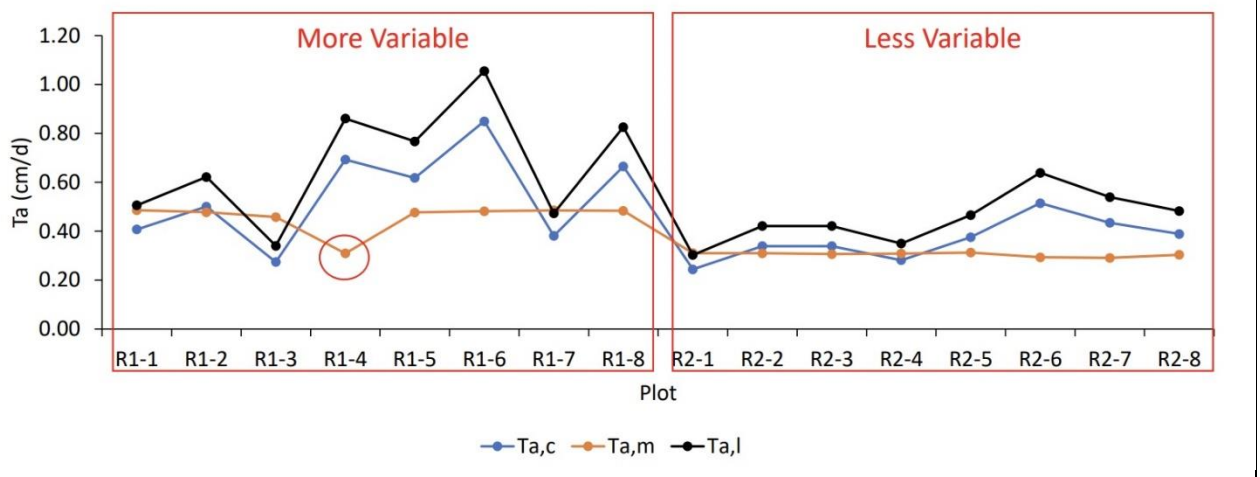

Figure 21. The Leaf-scale transpiration rates (black line), $T_{a,l}$, the canopy-scale transpiration rates (blue line), $T_{a,c}$, and the transpiration rates calculated by FLOWS-HAGES agro-hydrological model (orange line), $T_{a,m}$, for the 16 plots. Plot names starting with R1 refer to the control plots while those starting with R2 refer to the plots with deficit irrigation.

Field measurements can only be carried out at a limited number of times while the Agro-hydrological model's strength point is that it can provide information on the root water uptake, and subsequently the transpiration over the entire growth season provided the proper calibration of the model, its output can be more useful for irrigation management. In addition, the model can also predict root water uptake at any depth in the root zone.

3.5. Analysing the correlation among soil hydraulic parameters and crop parameters

3.5.1. Relationship between canopy-level transpiration rates and the soil hydraulic parameters

Figure 22 shows the $T_{a,c}$ rates predicted by Multiple Linear Regression, MLR, plotted against the $T_{a,c}$ rates obtained by upscaling the leaf-scale transpiration rates. The root-mean-square error, RMSE, was 0.12 cm/d. The coefficient of correlation, *R*, was 0.67. Table 2 shows the intercept and the coefficients of the normalized soil hydraulic parameters, SHP, used in the MLR to predict the $T_{a,c}$ rates. Before carrying out the MLR analysis, the parameters were normalized by dividing each parameter by its mean value. The table indicates that the parameters *n* and θ_s significantly affect the upscaled, canopy-scale, transpiration rates.

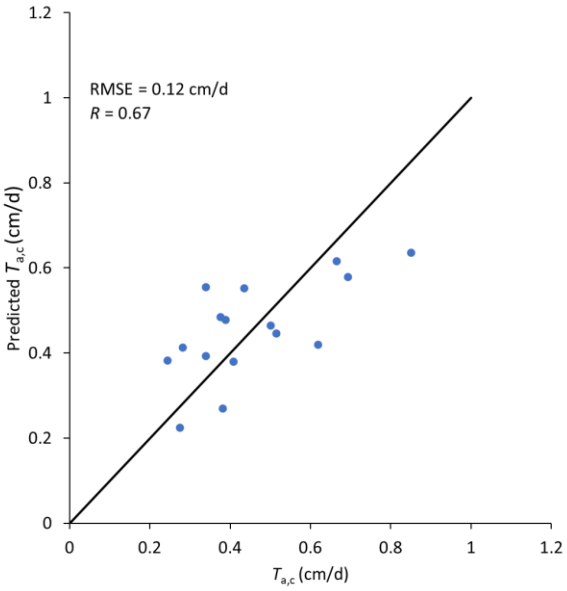

Figure 22. The $T_{a,c}$ rates predicted by MLR using the normalized SHP, plotted against the $T_{a,c}$ rates obtained by upscaling the leaf-scale transpiration rates. The RMSE, and R are reported in this figure. The blue circle markers represent all 16 plots.

Table 2. The MLR intercepts and coefficients of the normalized SHP, to obtain the canopy-scale transpiration rates, $T_{a,c}$

Normalized Parameter	$T_{a,c}$ *
Intercept	-18.93
θ_s	2.15
α	-0.06
n	17.34
K_s (cm/day)	-0.04

3.5.2. Relationship between transpiration rates obtained by FLOWS-HAGES, the soil hydraulic parameters and the canopy-scale stomatal conductance

Figure 23 shows the $T_{a,m}$ rates predicted by MLR are plotted against the $T_{a,m}$ rates obtained by FLOWS-HAGES, using the normalized SHP. The root-mean-square error, RMSE, was 0.08 cm/d. The coefficient of correlation, *R*, was 0.43.

Table 3 shows the intercept and the coefficients of the normalized SHP used in the MLR to predict $T_{a,m}$.

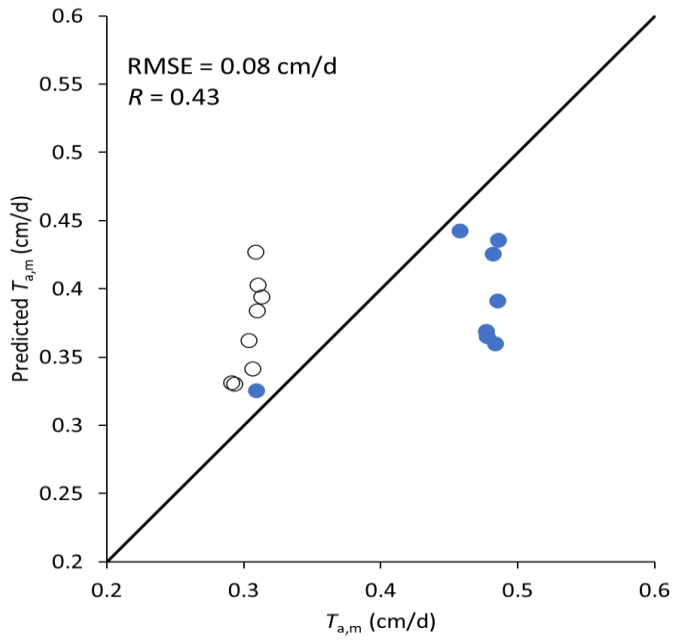

Figure 23. The $T_{a,m}$ rates predicted by MLR are plotted against the $T_{a,m}$ rates obtained by FLOWS-HAGES using the normalized SHP. The figure also reports the RMSE and *R*. The blue circle markers represent the control group (R1 plots) and the black markers represent the group with deficit irrigation (R2 plots).

Table 3. The MLR, intercepts, and coefficients of the SHP to obtain the macroscopic transpiration rates obtained by FLOWS-HAGES, $T_{a,m}$

Normalized Parameter	$T_{a,c}$ *
Intercept	-5.59
θ_s	0.13
α	0.03
n	5.75
K_s (cm/day)	0.06

Table 3 shows that $T_{a,m}$ is strongly affected by the parameters n_{vG} and the saturated water content θ_s. Nevertheless, the low value of the coefficient of correlation in Figure 23 indicates that the soil hydraulic parameters do not contain enough information to sufficiently predict the macroscopic transpiration rates.

Figure 24 shows the $T_{a,m}$ rates predicted by MLR plotted against the $T_{a,m}$ rates obtained by FLOWS-HAGES, using the normalized soil hydraulic parameters, SHP and the normalized canopy-scale

stomatal conductance, $g_{s,c}$. The figure also reports the Root Mean Square Error, RMSE, and the correlation coefficient, *R*. The blue circle markers represent the control group (R1 plots) and the black markers represent the group with deficit irrigation (R2 plots). Table 4 reports the multiple linear regression, MLR, intercept and coefficients of the normalized soil hydraulic parameters, SHP, and the normalized canopy-scale stomatal conductance, $g_{s,c}$, to obtain the macroscopic transpiration rates obtained by FLOWS-HAGES, $T_{a,m}$.

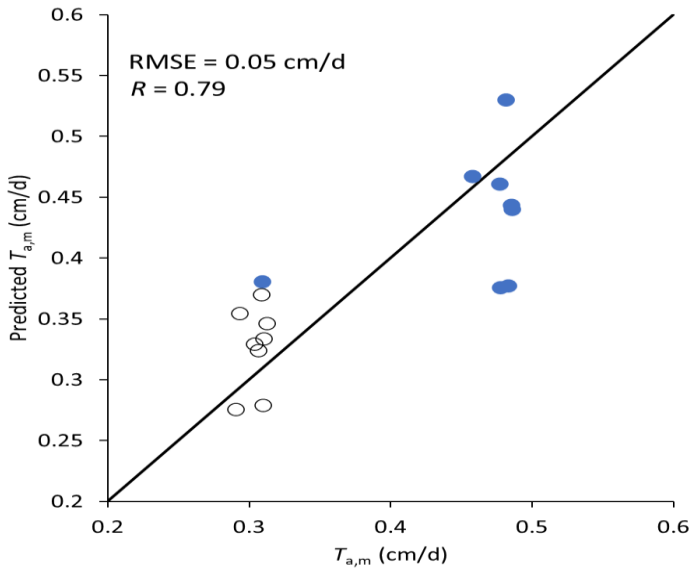

Figure 24. The $T_{a,m}$ rates predicted by MLR are plotted against the $T_{a,m}$ rates obtained by FLOWS-HAGES, using the SHP and the normalized $g_{s,c}$. The figure also reports the RMSE, and the *R*. The blue circle markers represent the control group (R1 plots) and the black markers represent the group with deficit irrigation (R2 plots).

Table 4. The MLR, intercept and coefficients of the normalized SHP, and the normalized $g_{s,c}$, to obtain the macroscopic transpiration rates obtained by FLOWS-HAGES, $T_{a,m}$

Normalized Parameter	$T_{a,c}$ *
Intercept	3.18
θ_s	-0.78

α	0.06
n	-2.36
K_s (cm/day)	0.08
$g_{s,c}$	0.20

Looking at Figure 24, the MLR ability to predict $T_{a,m}$ improved by introducing $g_{s,c}$. This was confirmed by the improved values of RMSE and R which were 0.05 cm/d and 0.79, respectively. Also, Table 4 confirms that $T_{a,m}$ is strongly affected by the parameters n_{vG} and the saturated water content θ_s. In Figure 24, there are two clusters of points: i) the values to the lower left representing the plots with deficit irrigation as well as the plot R1-4, and ii) the values to the upper right representing the plots with full irrigation except for plot R1-4. The low transpiration rates at plot R1-4 can be explained in Table *1*; plot R1-4 had the least conductive soil with the lowest value of K_s at 18.974 cm/d. The low conductivity in plot R1-4 led to the accumulation of water in the root zone and, subsequently, increased the soil water pressure head above the field capacity. In fact, the soil water pressure head frequently reached saturation as shown in Figure 25.

Figure 25 shows: the upper part (a): the evolution of the average soil-water pressure head in the root zone obtained by FLOWS-HAGES model for the plots R1-1 (solid line) and R1-4 (dashed line) during the growth season; and the lower part (b): the Feddes (1978) water stress response function used in this study; when the soil-water pressure head has a value above -1 cm, the stress coefficient, α_{rw}, decreases due to oxygen deficit.

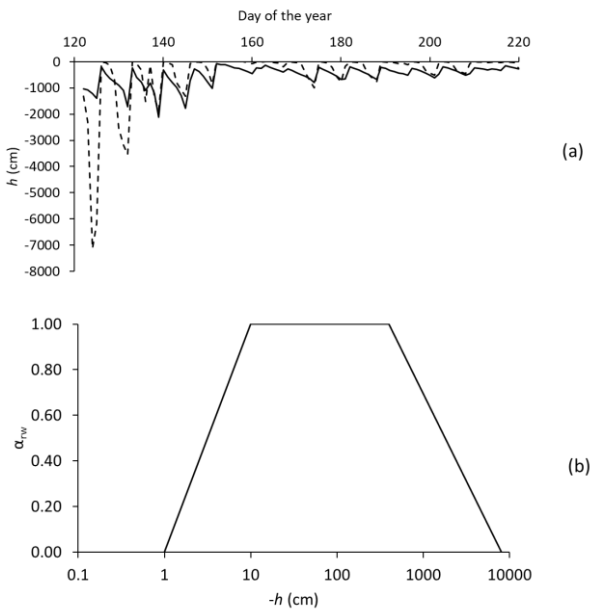

Figure 25. The upper part (a) is the evolution of the average soil-water pressure head in the root zone obtained by FLOWS-HAGES model for the plots R1-1 (solid line) and R1-4 (dashed line) during the growth season. The lower part (b) is the Feddes (1978) water stress response function used in this study; when the soil-water pressure head has a value above -1 cm, the stress coefficient, α_{rw}, decreases due to oxygen deficit.

Chapter 4

4. Conclusions and future perspectives

The main purpose of this dissertation was to compare the actual transpiration rates as measured at the microscopic leaf scale and as calculated by an agro-hydrological model at the macroscopic scale. It also studied the relationship between the actual transpiration rates and the variability of soil hydraulic properties under full irrigation and deficit irrigation.

Water uptake is a key component of the soil hydrological balance and is of concern for a range of hydrological, agricultural and ecological applications, as it controls, either directly or indirectly, the partitioning of infiltrating water into evaporation, transpiration and deep percolation fluxes. It is a dynamic process influenced by soil, plant and climate conditions. It depends on a number of factors such as soil water pressure head, soil hydraulic conductivity, osmotic head (in saline condition), evaporative demand, rooting depth, root density distribution and plant properties.

The study mostly focused on the role of soil hydraulic properties in root water uptake and, subsequently, transpiration rates. This emphasis was shown in the Multiple Linear Regression, MLR, results for both canopy transpiration upscaled from leaf-scale measurements and the macroscopic transpiration rates obtained from the agro-hydrological model FLOWS.

Transpiration measurements are needed for large-scale applications like irrigation management, and understanding the crop response to fertilizers, irrigation, etc. The measurement system problems are mostly related to the cost, the high spatial variability (e.g., leaf-scale measurements), or lack thereof (e.g., eddy covariance). Another problem is that transpiration measurements are not able to provide information about the actual transpiration and the soil hydraulic properties. Agro-hydrological modelling overcomes these problems as shown in the results.

Measurement systems account only for the T_a in the observation area without accounting for the spatial variability of the soil hydraulic properties and their effect on T_a. Systems like Eddy covariance

and IRGAs only account for the canopy cover and not the relationship between T_a and the soil-water availability (soil-water pressure head in the root zone). When it comes to spatial variability, the measurements can have one of two problems: 1) the erratic spatial variability coming from leaf-scale measurements which results from the canopy structure, the choice of leaves, and other factors.; and 2) the impossibility to discriminate T_a rates between experimental plots when their size is smaller than the observation window covered by the measurement system such as the eddy covariance system whose footprint covers a distance of at least 100 - 200 m from the measurement station. Agro-hydrological models provide a suitable compromise; they can provide information on T_a rates over the whole growth season which can be difficult by leaf-scale measurements. It also provides information on the spatial variability of T_a rates once it is adequately calibrated. Another advantage of agro-hydrological models is their ability to find the effect of the variability of soil hydraulic properties on the T_a rates based on the soil-water availability represented by the soil-water pressure head in the root zone.

Overall, agro-hydrological models allow physically based descriptions of plant water uptake, and thus of transpiration, based on the observed response to both soil water pressure and osmotic potentials. However, in using these models, one should be always aware that the macroscopic approach is essentially an empirical approach and needs to be calibrated for different plants and climatic conditions. This call for appropriate monitoring for a correct calibration and validation of the root uptake parameters under different soil water and salinity conditions. Any model applications not based on a preliminary and robust calibration and validation of the different process parameters involved remains only an academic exercise.

References

1. Abrahamsen P., Hansen S. 2000. Daisy: an open soil-crop-atmosphere system model. Environ. Modell. Softw. 15(3): 313–330. doi: https://doi.org/10.1016/S1364-8152(00)00003-7
2. Ankeny M.D., Kaspar T.C., Horton R. 1988. Design for an automated tension infiltrometer. Soil Sci. Soc. Am. J. 52(3): 893-896.
3. Arnold, M.A., & Mcdonald, G., 2009. Groundcovers, Organic and Inorganic Mulches, and Masonry Surfaces Differentially Affect Establishment and Root Zone Characteristics of Urban Trees. Arboriculture & Urban Forestry 35(5): 232–240. DOI:10.48044/jauf.2009.037
4. Arya L.M., Paris J.F. 1981. A physicoempirical model to predict the soil moisture characteristic from particle-size distribution and bulk density data. Soil Sci. Soc. Am. J. 45(6): 1023-1030.
5. Aslyng, H.C., 1963. Soil physics terminology. Int. Soc. Soil Sci. Bull, 23(7), p.321.
6. Babalola O., Fawusi M.O.A. 1980. Drought susceptibility of two tomato (Lycopersicum esculentum) varieties. Plant Soil. 55(2): 205–214. doi: 10.1007/BF02181800
7. Babalola, O. and Fawusi, M.O.A., 1980. Drought susceptibility of two tomato (Lycopersicum esculentum) varieties. Plant and Soil, 55(2), pp.205-214. https://doi.org/10.1007/BF02181800
8. Baldocchi D., Meyers T. 1998. On using eco-physiological, micrometeorological and biogeochemical theory to evaluate carbon dioxide, water vapor and trace gas fluxes over vegetation: a perspective. Agr. Forest Meteorol. 90(1): 1–25. doi: https://doi.org/10.1016/S0168-1923(97)00072-5
9. Barrios-Masias, F.H., Knipfer, T. and McElrone, A.J., 2015. Differential responses of grapevine rootstocks to water stress are associated with adjustments in fine root hydraulic physiology and suberization. Journal of Experimental Botany, 66(19), pp.6069-6078. https://doi.org/10.1093/jxb/erv324
10. Barrios-Masias, F.H.; Jackson, L.E. Increasing the effective use of water in processing tomatoes through alternate furrow irrigation without a yield decrease. Agric. Water Manag. 2016, 17, 107–

117.

11. Battilani, A., Letterio, T. and Chiari, G., 2014, June. AquaCrop model calibration and validation for processing tomato crop in a sub-humid climate. In XIII International Symposium on Processing Tomato 1081 (pp. 167-174). DOI: 10.17660/ActaHortic.2015.1081.19
12. Belviso C., Satriani A., Lovelli S., Comegna A., Coppola A., Dragonetti G., Cavalcante F., Rivelli A.R. 2022. Impact of zeolite from coal fly ash on soil hydrophysical properties and plant growth. Agriculture. 12: 356. doi: https://doi.org/10.3390/agriculture12030356.
13. Blum, A., 2009. Effective use of water (EUW) and not water-use efficiency (WUE) is the target of crop yield improvement under drought stress. Field crops research, 112(2-3), pp.119-123. https://doi.org/10.1016/j.fcr.2009.03.009
14. Bouma J. 1987. Transfer functions and threshold values: from soil characteristics to land qualities. Workshop on Quantified Land Evaluation Process. International Institute for Aerosphere Survey and Earth Science, Washington, D.C., USA, 6: 106-110
15. Boyer, J.S., 1995. Measuring the water status of plants and soils. Academic Press, Inc. http://udspace.udel.edu/handle/19716/2828
16. Brisson N., Itier B., L'Hotel J.C., Lorendeau J.Y. 1998. Parameterisation of the Shuttleworth-Wallace model to estimate daily maximum transpiration for use in crop models. Ecol. Model. 107(2): 159–169. doi: https://doi.org/10.1016/S0304-3800(97)00215-9
17. Buck A.L. 1981. New equations for computing vapor pressure and enhancement factor. J. Appl. Meteorol. Clim. 20(12): 1527–1532. doi: 10.1175/1520-0450(1981)020<1527:NEFCVP>2.0.CO;2
18. Buckingham, E. (1907) Studies on the Movement of Soil Moisture. published as Bulletin 38 of the. U.S. Department of Agriculture Bureau of Soils, Washington D.C. 61 pp.
19. Buckley T.N., Mott K.A. 2002. Dynamics of stomatal water relations during the humidity response: implications of two hypothetical mechanisms. Plant Cell Environ. 25(3): 407–419. doi: https://doi.org/10.1046/j.0016-8025.2001.00820.x

20. Canadell, J., Jackson, R.B., Ehleringer, J.B. et al. Maximum rooting depth of vegetation types at the global scale. Oecologia 108, 583–595 (1996). https://doi.org/10.1007/BF00329030
21. Cantero-Navarro, E., Romero-Aranda, R., Fernández-Muñoz, R., Martínez-Andújar, C., Pérez-Alfocea, F. and Albacete, A., 2016. Improving agronomic water use efficiency in tomato by rootstock-mediated hormonal regulation of leaf biomass. Plant Science, 251, pp.90-100. https://doi.org/10.1016/j.plantsci.2016.03.001
22. Cantore V., Iovino F. and Pontecorvo G., 1987. Aspetti climatici e zone fitoclimatiche della Basilicata. CNR IEIF-Cosenza, Grafiche Badiali s.n.c. (ed.), Arezzo, 2, 49 p.
23. Čereković N., Todorović M., Snyder R.L. 2010. The relationship between leaf area index and crop coefficient for tomato crop grown in Southern Italy. Euroinven. 1(1): 3–10.
24. Comegna A., Coppola A., Dragonetti G. 2019. A soil non-aqueous phase liquid (NAPL) flushing laboratory experiment based on measuring the dielectric properties of soil–organic mixtures via time domain reflectometry (TDR). Hydrol. Earth Syst. Sci. 23: 3593-3602. Doi: https://doi. org/10.5194/hess-23-3593-2019.
25. Comegna A., Coppola A., Dragonetti G. 2020. Time domain reflectometry for dielectric characterization of olive mill wastewater contaminated soils. J. Agr. Eng. 51(4): 248-254. Doi: https://doi. org/10.4081/jae.2020.1092.
26. Comegna A., Coppola A., Dragonetti G., Severino G., Sommella A., Basile A. 2013. Dielectric properties of a tilled sandy volcanic-vesuvian soil with moderate andic features. Soil till. Res. 133: 93-100. Doi: https://doi. org/ 10. 1016/j. still. 2013. 06. 003.
27. Comegna A., Coppola A., Dragonetti G., Sommella A. 2016. Estimating non-aqueous phase liquid content in variably saturated soils using time domain reflectometry. Vadose Zone J. 15(5): 1-11. doi: https://doi.org/10.2136/vzj2015.11.0145.
28. Comegna A., Coppola A., Dragonetti G., Sommella A. 2017. Interpreting TDR signal propagation through soils with distinct layers of nonaqueous-phase liquid and water content. Vadose Zone J. 16(13): 1-11. doi: https://doi. org/ 10. 2136/ vzj20 17. 07. 0141.

29. Comegna A., Dragonetti G., Kodesova R., Coppola A., 2022b. Impact of olive mill wastewater (OMW) on the soil hydraulic and solute transport properties. Int. J. Environ. Sci. Te. 19: 7079-7092. Doi: https://doi.org/10.1007/s13762-021-03630-6.

30. Comegna A., Severino G., Coppola A., 2022a. A review of new TDR applications for measuring non-aqueous phase liquids (NAPLs) in soils. Environ. Adv. 9: 100296. Doi: https://doi.org/10.1016/j.envadv.2022.100296.

31. Coppola A., Chaali N., Dragonetti G., Lamaddalena N., Comegna A. 2015. Root uptake under non-uniform root-zone salinity. Ecohydrology. 8(7): 1363–1379. doi: 10.1002/eco.1594

32. Coppola A., Comegna A., Dragonetti G., Dyck M., Basile A., Lamaddalena N., Kassab M., Comegna V. 2011. Solute transport scales in an unsaturated stony soil. Adv. Water Resour. 34: 747-759.

33. Coppola A., Dragonetti G., Moghrani S., Hassan S.B.M., Comegna A., 2022. A fast and simple method to measure soil hydraulic properties in multiple sites. Submitted to Vadose Zone J.

34. Coppola A., Dragonetti G., Sengouga A., Lamaddalena N., Comegna A., Basile A., Noviello N., Nardella L. 2019. Identifying optimal irrigation water needs at district scale by using a physically based agro-hydrological model. Water. 11(4): 841-865. doi: 10.3390/w11040841

35. Coppola A., Smettem K., Ajeel A., Saeed A., Dragonetti G., Comegna A., Lamaddalena N., Vacca A. 2016. Calibration of an electromagnetic induction sensor with time-domain reflectometry data to monitor rootzone electrical conductivity under saline water irrigation. Eur. J. Soil Sci. 67(6): 737-748.

36. Cowan I.R., Farquhar G.D. 1977. Stomatal function in relation to leaf metabolism and environment. Sym. Soc. Exp. Biol. 31: 471–505

37. Cowan, I.R., 1965. Transport of water in the soil-plant-atmosphere system. Journal of Applied Ecology, pp.221-239.

38. Darcy, H., 1856. Les fontaines publiques de la ville de Dijon: Exposition et application des principes à suivre et des formules à employer dans les questions de distribution d'eau: Ouvrage

terminé par un appendice relatif aux fournitures d'eau de plusieurs villes, au filtrage des eaux et à la fabrication des tuyaux de fonte, de plomb, de tôle et de bitume (Vol. 2). V. Dalmont.

39. Davis, S.D. and Mooney, H.A. (1986) Water use patterns of four co-occurring chaparral shrubs. Oecologia 70: 172-177.
40. Dewar R.C. 2002. The Ball–Berry–Leuning and Tardieu–Davies stomatal models: synthesis and extension within a spatially aggregated picture of guard cell function. Plant Cell Environ. 25(11): 1383–1398. doi: https://doi.org/10.1046/j.1365-3040.2002.00909.x
41. DOI: 10.1029/WR026i009p02119
42. Dragonetti G., Comegna A., Ajeel A., Deidda G.P., Lamaddalena N., Rodriguez G., Vignoli G., Coppola A. 2018. Calibrating electromagnetic induction conductivities with time domain reflectometry measurements. Hydrol. Earth Syst. Sci. 22(2): 1509-1523.
43. Dragonetti G., Farzamian M., Basile A., Santos F.M., Coppola A. 2022. In situ estimation of soil hydraulic and hydrodispersive properties by inversion of electromagnetic induction measurements and soil hydrological modeling. Hydrol. Earth Syst. Sci. 26(19): 5119-5136.
44. Du, S., Kang, S., Li, F. and Du, T., 2017. Water use efficiency is improved by alternate partial root-zone irrigation of apple in arid northwest China. Agricultural Water Management, 179, pp.184-192.https://doi.org/10.1016/j.agwat.2016.05.011
45. Eviner, V.T., Stuart Chapin, F., 2002. The influence of plant species, fertilization and elevated CO2 on soil aggregate stability. Plant and Soil 246, 211–219. https://doi.org/10.1023/A:1020657107687
46. FAO (Food and Agriculture Organization of the United Nations), FAOSTAT database, accessed January 15, 2017. www.fao.org/faostat/.
47. Feddes R.A. 1978. Simulation of field water use and crop yield. PUDOC, Waginengen, The Netherlands. Page 189
48. Feddes R.A., Raats P.A.C. 2004. Parameterizing the soil - water - plant root system. In: Feddes R. A., de Rooij G. H., van Dam J. C. (Eds.). Unsaturated-zone modeling; Progress, challenges

and applications, Wageningen UR Frontis Series : 6. 74, Kluwer Academic Publishers, Dordrecht, The Netherlands, pp. 95–141.

49. Feddes, R.A., Hoff, H., Bruen, M., et al., 2001. Modeling root water uptake in hydrological and climate models. Bulletin of the American Meteorological Society, 82 (12), 2797-2809. DOI: https://doi.org/10.1175/1520-0477(2001)082<2797:MRWUIH>2.3.CO;2
50. Feddes, RA & Raats, PAC 2004, Parameterizing the soil - water - plant root system. in RA Feddes, GH de Rooij & JC van Dam (eds), Unsaturated-zone modeling; Progress, challenges and applications. Wageningen UR Frontis Series, no. 6, Dordrecht, pp. 95-141. https://edepot.wur.nl/35358
51. Fereres, E. and Soriano, M.A., 2007. Deficit irrigation for reducing agricultural water use. Journal of experimental botany, 58(2), pp.147-159.https://doi.org/10.1093/jxb/erl165
52. Frusciante L., Barone A., Carputo D., Ercolano M.R., della Rocca F., Esposito S. 2000. Evaluation and use of plant biodiversity for food and pharmaceuticals. Fitoterapia, 71: S66–S72. doi: https://doi.org/10.1016/S0367-326X(00)00175-1
53. Frusciante, L., Barone, A., Carputo, D., Ercolano, M.R., della Rocca, F. and Esposito, S., 2000. Evaluation and use of plant biodiversity for food and pharmaceuticals. Fitoterapia, 71, pp.S66-S72. https://doi.org/10.1016/S0367-326X(00)00175-1
54. Gardner, W.R., 1960. Dynamic aspects of water availability to plants. Soil science, 89(2), pp.63-73.
55. Geerts, S. and Raes, D., 2009. Deficit irrigation as an on-farm strategy to maximize crop water productivity in dry areas. Agricultural water management, 96(9), pp.1275-1284. https://doi.org/10.1016/j.agwat.2009.04.009
56. Hassan S.B.M., Dragonetti G., Comegna A., Sengouga A., Lamaddalena N., Coppola A. 2022. A bimodal extension of the ARYA&PARIS approach for predicting hydraulic properties of structured soils. J. Hydrol. 610: 127980.
57. Heidi Asbjornsen, Gregory R. Goldsmith, Maria S. Alvarado-Barrientos, Karin Rebel, Floortje

P. Van Osch, Max Rietkerk, Jiquan Chen, Sybil Gotsch, Conrado Tobón, Daniel R. Geissert, Alberto Gómez-Tagle, Kellie Vache, Todd E. Dawson, 2011. Ecohydrological advances and applications in plant–water relations research: a review, *Journal of Plant Ecology*, Volume 4, Issue 1-2. Pages 3–22, https://doi.org/10.1093/jpe/rtr005

58. Hildebrandt, A., and E. A. B. Eltahir, 2007. Ecohydrology of a seasonal cloud forest in Dhofar: 2. Role of clouds, soil type, and rooting depth in tree-grass competition, Water Resour. Res., 43, W11411, doi:10.1029/2006WR005262.
59. Hillel, D., Beek, V. and Talpaz, H., 1975. A microscopic-scale model of soil water uptake and salt movement to plant roots. Soil Science, 120(5), pp.385-399.
60. Homaee, M., Dirksen, C. and Feddes, R.A., 2002. Simulation of root water uptake: I. Non-uniform transient salinity using different macroscopic reduction functions. Agricultural Water Management, 57(2), pp.89-109. https://doi.org/10.1016/S0378-3774(02)00072-0
61. Homaee, M., Feddes, R.A. and Dirksen, C., 2002. Simulation of root water uptake: II. Non-uniform transient water stress using different reduction functions. Agricultural water management, 57(2), pp.111-126. https://doi.org/10.1016/S0378-3774(02)00071-9
62. Hopmans, J.W., & Bristow, K.L. (2002). Current Capabilities and Future Needs of Root Water and Nutrient Uptake Modeling. Advances in Agronomy, 77, 103-183. DOI: 10.1016/S0065-2113(02)77014-4
63. Hui, Y., Hongxia, C., Xinmei, H., Lijie, G., Hongzheng, L. and Xuanyi, W., 2017. Evaluation of tomato fruit quality response to water and nitrogen management under alternate partial root-zone irrigation. International Journal of Agricultural and Biological Engineering, 10(5), pp.85-94. DOI: 10.25165/j.ijabe.20171005.2622
64. Jackson, R. B., J. Canadell, J. R. Ehleringer, H. A. Mooney, O. E. Sala, and E. D. Schulze, 1996. A global analysis of root distributions for terrestrial biomes, Oecologia, 108, 389 – 411.
65. Jackson, R.B., Anderson, L.J. and Pockman, W.T., 2000. Measuring water availability and uptake in ecosystem studies. In Methods in ecosystem science (pp. 199-214). Springer, New

York, NY. DOI: 10.1007/978-1-4612-1224-9_14

66. Jackson, R.B., Sperry, J.S. and Dawson, T.E., 2000. Root water uptake and transport: using physiological processes in global predictions. Trends in plant science, 5(11), pp.482-488. https://doi.org/10.1016/S1360-1385(00)01766-0
67. Jarvis P.G., McNaughton K.G. 1986. Stomatal control of transpiration: Scaling up from leaf to region. In: MacFadyen A., Ford E.D. (Eds.) Advances in ecological research. Vol. 15, Academic Press, London, UK, pp. 1–49. doi: https://doi.org/10.1016/S0065-2504(08)60119-1
68. Jarvis P.G., Monteith J.L., Weatherley P.E. 1976. The interpretation of the variations in leaf water potential and stomatal conductance found in canopies in the field. Philos. T. Roy. Soc. B. 273(927): 593–610. doi: 10.1098/rstb.1976.0035
69. Knight J.H. White I. Zegelin S.J. 1995. Sampling volume of TDR probes used for water content monitoring. Proc. Symp. Workshop on Time Domain Reflectometry in Env. Infrastruct. Min, Appl. Evanston, IL, USA, SP 19-94: 93-104
70. Knipfer, T. and Fricke, W., 2011. Water uptake by seminal and adventitious roots in relation to whole-plant water flow in barley (Hordeum vulgare L.). Journal of experimental botany, 62(2), pp.717-733. https://doi.org/10.1093/jxb/erq312
71. Koorevaar, P., Menelik, G. and Dirksen, C., 1983. Elements of soil physics. Elsevier. 227 pp.
72. Kreszies, T., Schreiber, L. and Ranathunge, K., 2018. Suberized transport barriers in Arabidopsis, barley and rice roots: from the model plant to crop species. Journal of Plant Physiology, 227, pp.75-83. https://doi.org/10.1016/j.jplph.2018.02.002
73. Lambers, H., Chapin, F.S. and Pons, T.L., 2008. Plant physiological ecology (Vol. 2, pp. 11-99). New York: Springer.
74. Le Roux, X., Abbadie, L., Lensi, R. and Serça, D., 1995. Emission of nitrogen monoxide from African tropical ecosystems: Control of emission by soil characteristics in humid and dry savannas of West Africa. Journal of Geophysical Research 100: doi: 10.1029/95JD01923. issn: 0148-0227.

75. Leuning, R., Kelliher, F. M., De Pury, D. G. G., & Schulze, E. D., 1995. Leaf nitrogen, photosynthesis, conductance and transpiration: scaling from leaves to canopies. Plant, Cell & Environment, 18(10), 1183-1200.

76. Li X., Yang P., Ren S., Li Y., Liu H., Du J., Li P., Wang C., Ren L. 2010. Modeling cherry orchard evapotranspiration based on an improved dual-source model. Agr. Water Manage. 98(1): 12–18. doi: https://doi.org/10.1016/j.agwat.2010.07.019

77. Meißner, M., Köhler, M., Schwendenmann, L., Hölscher, D., & Dyckmans, J., 2014. Soil water uptake by trees using water stable isotopes (δ^2H and $\delta\ ^{18}O$)—a method test regarding soil moisture, texture and carbonate. Plant and Soil, 376, 327–335. https://doi.org/10. 1007/s11104-013-1970-z

78. Mmolawa, K. and Or, D., 2000. Root zone solute dynamics under drip irrigation: A review. Plant and soil, 222(1), pp.163-190. https://doi.org/10.1023/A:1004756832038

79. Molz F.J. 1981. Models of water transport in the soil-plant system: A review. Water Resour. Res. 17(5): 1245–1260. doi: https://doi.org/10.1029/WR017i005p01245

80. Molz F.J. 1981. Models of water transport in the soil-plant system: A review. Water Resour. Res. 17(5): 1245–1260. doi: https://doi.org/10.1029/WR017i005p01245

81. Molz, F. J., I. Remson, A. A. Fungaroli, and R. L. Drake, Soil moisture availability for transpiration, Water Resour. Res., 4(6), 1161-1169, 1968. https://doi.org/10.1029/WR004i006p01161

82. Molz. F.J. 1981. Models of water transport in the soil-plant system: A review. Water Resour. Res. 17:1245-1260. https://doi.org/10.1029/WR017i005p01245

83. Monteith J., Unsworth M. 2013. Principles of environmental physics: plants, animals, and the atmosphere. 4th ed. Academic Press, Oxford, UK.

84. Moran, M. S., Rahman, A. F., Washburne, J. C., Goodrich, D. C., Weltz, M. A., & Kustas, W. P., 1996. Combining the Penman-Monteith equation with measurements of surface temperature and reflectance to estimate evaporation rates of semiarid grassland. Agricultural and forest

Meteorology, 80(2-4), 87-109.

85. Mu Q., Zhao M., Running S.W. 2011. Improvements to a MODIS global terrestrial evapotranspiration algorithm. Remote Sens. Environ. 115(8): 1781–1800. doi: https://doi.org/10.1016/j.rse.2011.02.019
86. Parkinson K.J. 1983. Porometry in S.E.B. Symp. instrumentation for environmental physiology, Cambridge, UK.
87. Passioura, J.B., 1988. Water transport in and to roots. Annual Review of Plant Physiology and Plant Molecular Biology, 39(1), pp.245-265.
88. Peet, M.M., 2005. Irrigation and fertilization. Crop production science in horticulture, 13, p.171.
89. PP Systems. 2017. CIRAS-3 Portable photosynthesis system operation manual. Version 1. PP Systems, Amesbury, Massachusetts, US.
90. Richards, R.A. and Passioura, J.B., 1989. A breeding program to reduce the diameter of the major xylem vessel in the seminal roots of wheat and its effect on grain yield in rain-fed environments. Australian Journal of Agricultural Research, 40(5), pp.943-950. https://doi.org/10.1071/AR9890943
91. Roose T., Fowler A.C. 2004. A model for water uptake by plant roots. J. Theor. Biol. 228(2): 155–171. doi: https://doi.org/10.1016/j.jtbi.2003.12.012
92. Roose, T. and Fowler, A.C., 2004. A model for water uptake by plant roots. Journal of Theoretical Biology, 228(2), pp.155-171. https://doi.org/10.1016/j.jtbi.2003.12.012
93. Rudich J., Kalmar D., Geizenberg C. and Harel S. 1977. Low water tensions in defined growth stages of processing tomato plants and their effects on yield and quality. J. Hortic. Sci. 52(3): 391–399. doi: 10.1080/00221589.1977.11514768
94. Rudich, J., Kalmar, D., Geizenberg, C. and Harel, S., 1977. Low water tensions in defined growth stages of processing tomato plants and their effects on yield and quality. Journal of Horticultural Science, 52(3), pp.391-399. https://doi.org/10.1080/00221589.1977.11514768
95. Russell, R.S., 1977. Plant root systems: their function and interaction with the soil. McGraw-Hill

Book Company (UK) Limited. 298pp

96. Russo D., 1988. Determining soil hydraulic properties by parameter estimation: On the selection of a model for the hydraulic properties. Water Resour. Res. 24(3): 453-459.
97. Schaap M.G., Robinson D.A., Friedman S.P., Lazar A. 2003. Measurement and modeling of the TDR signal propagation through layered dielectric media. Soil Sci Soc Am J. 61(4): 1113-1121.
98. Schmidhalter U, Selim H M and Oertli J J 1994Measuring and modeling root water uptake based on chloride discrimination in a silt loam soil affected by groundwater. Soil Sci. 158, 97–105.DOI: 10.1097/00010694-199408000-00003
99. Schröder T., Javaux M., Vanderborght J., Körfgen B., Vereecken H. 2008. Effect of local soil hydraulic conductivity drop using a three-dimensional root water uptake model. Vadose Zone J. 7(3): 1089–1098. doi: https://doi.org/10.2136/vzj2007.0114
100. Shuttleworth W.J. 2007. Putting the “vap” into evaporation. Hydrol. Earth Syst. Sc. 11(1): 210–244. doi: 10.5194/hess-11-210-2007
101. Shuttleworth W.J., Wallace J.S. 1985. Evaporation from sparse crops-an energy combination theory. Q. J. Roy. Meteor. Soc. 111(469): 839–855. doi: https://doi.org/10.1002/qj.49711146910
102. Šimůnek J., van Genuchten M.T. 1996. Estimating unsaturated soil hydraulic properties from tension disc infiltrometer data by numerical inversion. Water Resour. Res. 32(9): 2683-2696.
103. Šimůnek J., van Genuchten M.T., Šejna M. 2008. Development and applications of the HYDRUS and STANMOD software packages and related codes. Vadose Zone J. 7(2): 587–600. doi: 10.2136/vzj2007.0077
104. Skaggs, T.H., Shouse, P.J. and Poss, J.A., 2006. Irrigating forage crops with saline waters: 2. Modeling root uptake and drainage. Vadose Zone Journal, 5(3), pp.824-837.https://doi.org/10.2136/vzj2005.0120
105. Skaggs, T.H., van Genuchten, M.T., Shouse, P.J. and Poss, J.A., 2006. Macroscopic approaches to root water uptake as a function of water and salinity stress. agricultural water management, 86(1-2), pp.140-149.https://doi.org/10.1016/j.agwat.2006.06.005

106. Steudle, E. and Peterson, C.A., 1998. How does water get through roots?. Journal of experimental Botany, 49(322), pp.775-788.https://doi.org/10.1093/jxb/49.322.775

107. Steudle, E. and Peterson, C.A., 1998. How does water get through roots?. Journal of experimental Botany, 49(322), pp.775-788. https://doi.org/10.1093/jxb/49.322.775

108. Thompson, A.J., Andrews, J., Mulholland, B.J., McKee, J.M., Hilton, H.W., Horridge, J.S., Farquhar, G.D., Smeeton, R.C., Smillie, I.R., Black, C.R. and Taylor, I.B., 2007. Overproduction of abscisic acid in tomato increases transpiration efficiency and root hydraulic conductivity and influences leaf expansion. Plant physiology, 143(4), pp.1905-1917.https://doi.org/10.1104/pp.106.093559

109. Topp, G.C., Ferré, P.A. 2002. The soil solution phase. In: Dane J.H., Topp G.C., Campbell, G.S. (Eds.) Methods of soil analysis. Part 4. Physical methods. SSSA Book series No. 5, Madison, WI, USA, pp. 417-545.

110. van Dam J.C., Huygen J., Wesseling J.G., Feddes R.A., Kabat P., van Walsum P.E. V, Groenendijk P., van Diepen C.A. 1997. Theory of SWAP version 2.0; Simulation of water flow, solute transport and plant growth in the soil-water-atmosphere-plant environment. Technical Doc. 45. Wageningen Agricultural University and DLO Winand Staring Centre. Wageningen, The Netherlands

111. Van den Honert, T.H., 1948. Water transport in plants as a catenary process. Discussions of the Faraday Society, 3, pp.146-153.

112. Van Der Ploeg, M.J., Gooren, H.P., Bakker, G. and de Rooij, G.H., 2008. Matric potential measurements by polymer tensiometers in cropped lysimeters under water-stressed conditions. Vadose Zone Journal, 7(3), pp.1048-1054. https://doi.org/10.2136/vzj2007.0104

113. van Genuchten M.T. 1980. A closed-form equation for predicting the hydraulic conductivity of unsaturated soils. Soil Sci. Soc. Am. J. 44(5): 892–898. doi: https://doi.org/10.2136/sssaj1980.03615995004400050002x

114. von Caemmerer S., Farquhar G.D. 1981. Some relationships between the biochemistry of

photosynthesis and the gas exchange of leaves. Planta. 153(4): 376–387. doi: 10.1007/BF00384257

115. Wallach, R. & Van Genuchten, M.Th. 1990. A physically based model for predicting solute transfer from soil solution to rainfall-induced runoff water. Water Resources Research 26(9): 2119-2126

116. Wang E, Smith CJ (2004) Modeling the growth and water uptake function of plant root systems: a review. Australian Journal of Agricultural Research 55(5) 501-523 https://doi.org/10.1071/AR03201

117. Warrick A.W. 1974. Time-dependent linearized infiltration. I. Point sources. Soil Sci. Soc. Am. J. 38 (3): 383-386. doi: https://doi.org/10.2136/sssaj1974.03615995003800030008x

118. Wei, T., Dong, Z., Zhang, C., Ali, S., Chen, X., Han, Q., Zhang, F., Jia, Z., Zhang, P. and Ren, X., 2018. Effects of rainwater harvesting planting combined with deficiency irrigation on soil water use efficiency and winter wheat (Triticum aestivum L.) yield in a semiarid area. Field Crops Research, 218, pp.231-242. https://doi.org/10.1016/j.fcr.2017.12.019

119. Wilcox, B.P., Breshears, D.D. and Turin, H.J., 2003. Hydraulic conductivity in a piñon-juniper woodland: Influence of vegetation. Soil Science Society of America Journal, 67(4), pp.1243-1249. https://doi.org/10.2136/sssaj2003.1243

120. Williams M., Rastetter E.B., Fernandes D.N., Goulden M.L., Wofsy S.C., Shaver G.R., Melillo J.M., Munger J.W., Fa S.M., Nadelhoffer K.J. 1996. Modelling the soil-plant-atmosphere continuum in a Quercus–Acer stand at Harvard Forest: the regulation of stomatal conductance by light, nitrogen and soil/plant hydraulic properties. Plant, Cell & Environ. 19(8): 911–927. doi: https://doi.org/10.1111/j.1365-3040.1996.tb00456.x

121. Zhang, G., Liu, C., Xiao, C., Xie, R., Ming, B., Hou, P., Liu, G., Xu, W., Shen, D., Wang, K. and Li, S., 2017. Optimizing water use efficiency and economic return of super high yield spring maize under drip irrigation and plastic mulching in arid areas of China. Field Crops Research, 211, pp.137-146. https://doi.org/10.1016/j.fcr.2017.05.026

Chapter 5

5. Appendix

5.1. Appendix A. Analytical solution for transient flow from a point source method

The conventional method for describing multidimensional infiltration and subsequent distribution of water in a bare soil is to use Richard's equation:

$$C(h)\frac{\partial h}{\partial t} = \nabla(K(h)\nabla H) \qquad \text{A. 1}$$

where $C(h)=d\theta/dh$ [L^{-1}] is the soil water capacity, $H=z+h$ [L] is the total hydraulic head, h [L] is the soil water pressure head, z is the vertical coordinate being positive upward, t [T] is time, K(h) [$L\ T^{-1}$] is the soil hydraulic conductivity and ∇ is the Laplacian (the spatial gradient) operator.

Analytical solution of the equation 1 for both steady state and transient water flow may be obtained by a linearization procedure using the exponential hydraulic conductivity function proposed by Gardner (1958):

$$K(h) = K_s e^{\alpha_{GRD}} \qquad \text{A. 2}$$

where K_s is the saturated hydraulic conductivity (LT^{-1}), $\alpha_{GRD} = 1/\lambda_{GRD}$ where λ_{GRD} is a scaling parameter which quantifies the importance of capillary forces relative to gravity. Also, analytical solutions requires calculation of the so-called matrix flux potential, ϕ, defined as (Philip, 1968):

$$\phi(h) = \int_{-\infty}^{h} K(h)dh = \frac{K(h)}{\alpha_{GRD}} \qquad \text{A. 3}$$

Warrick (1974) solved the Richards equation analytically by using similar transformations (Eqs. A. 1 and A. 3) coupled with the additional assumption that $dK/d\theta = k$ or $d\theta/d\phi = \alpha_{GRD}/k$, where k is a constant, to linearize Richards Equation:

$$\frac{\partial \phi}{\partial t} = \frac{k}{\alpha_{GRD}} \nabla^2 \phi - k \frac{\partial \phi}{\partial z} \qquad \text{A. 4}$$

To solve Eq. A. 4 analytically, the dimensionless variables: $R = \alpha_{GRD} r/2$, $Z = \alpha_{GRD} z/2$, $T = \alpha_{GRD}\, kt/4$, $\rho = \sqrt{R^2 + Z^2}$, and the dimensionless matric flux potential: $\Phi_B = \alpha q \phi/8\pi$ were introduced, where r and z are spatial radial and vertical coordinates, and t is time. With the initial condition $\phi(r, z, 0) = 0$ and the boundary conditions $-\frac{\partial \phi}{\partial z} + \alpha_{GRD}\phi = 0$ for $z = 0, r \neq 0$, the analytical solution for a buried point source in an infinite medium is given as (Warrick, 1974):

$$\Phi_B(\mathrm{R}, \mathrm{Z}, \mathrm{T}) = \frac{e^z}{2\rho}\left[e^{\rho}\, erfc\left(\frac{\rho}{2\sqrt{T}} + \sqrt{T}\right) + e^{\rho}\, erfc\left(\frac{\rho}{2\sqrt{T}} - \sqrt{T}\right)\right] \qquad \text{A. 5}$$

where $erfc$ is the complementary error function given as (Spiegel and Liu, 1999):

$$erfc\,(x) = 1 - erfc\,(x) = \frac{2}{\sqrt{\pi}} \int_x^{\infty} e^{-u^2}\, du \qquad \text{A. 6}$$

The solution for a surface point source is:

$$\Phi_S(R, Z, T) = 2\left[\Phi_B - e^{2Z} \int_z^{\infty} e^{-2Z'} (\Phi_B)_{Z=Z'} dZ\right] \qquad \text{A. 7}$$

the integration of Eq. A. 7 can be accomplished by using the Gauss-Leguerre quadrature (Sen et al., 1992) :

$$\int_0^{\infty} e^{-2Z'} (\Phi_B)_{Z=Z'}\, dZ' = e^{-2Z} \int_0^{\infty} e^{-x}\, (\Phi_B)_{Z\prime=Z+x/2} \frac{dx}{2} \qquad \text{A. 8}$$

$$= \frac{1}{2} e^{-2Z} \sum_{i=0}^{x} \omega_i\, (\Phi_B)_{Z\prime=Z+x/2}$$

where Z' = Z+x/2. The weights ω_i and the sampling points x_i (for the 15-point formula used in this study) may be obtained from Carnahan *et al.* (1969).

For regular cyclic inputs (i.e., irrigation cycles) or other temporal variations in source strength, the value of Φ is obtained by superposition in time and knowing that $\Phi_B = \alpha q \phi / 8\pi$ (Warrick, 1974):

$$\phi(R,Z,T) = \frac{\alpha}{8\pi}\sum_{i=0}^{n}(q_i - q_{i-1})\ \Phi(R,Z,T-T_i) \qquad \begin{matrix} q_{-1}=0, T_0=0, T \\ > T_i \end{matrix} \qquad \text{A. 9}$$

Pressure head values can then be obtained from Eqs. A. 2 and A. 3 as:

$$h(r,z,t) = \frac{1}{\alpha_{GRD}} ln\left(\frac{\alpha_{GRD}\phi(r,z,t)}{K_s}\right) \qquad \text{A. 10}$$

Corresponding transient soil water content values $\theta(r,z,t)$ may be obtained by the soil water retention model proposed by Russo (1988):

$$S_e = \frac{\theta - \theta_r}{\theta_s - \theta_r} = [\exp(-0.5\alpha_{GR}h)(1+0.5\alpha_{GR}h)]^{\left(\frac{2}{\mu_R+2}\right)} \qquad \text{A. 11}$$

where α_{GR} is the soil parameter appearing in the Gardner's model for hydraulic conductivity related to the pore size distribution, while μ_R is a parameter related to tortuosity. *Se* is effective saturation and θ_s and θ_r are the water contents at h=0 and for $h \to \infty$, respectively. The choice of the Russo model comes from the fact that it is appropriate for the linearized equations as it is based on the same parameter α_{GR} used in the Gardner's exponential hydraulic conductivity function.